

Updated climatological mean delta fCO₂ and net sea–air CO₂ flux over the global open ocean regions

5 Amanda R. Fay¹, David R. Munro^{2,3}, Galen A. McKinley¹, Denis Pierrot⁴, Stewart C. Sutherland¹, Colm Sweeney³, Rik Wanninkhof⁴

Affiliations:

¹ Columbia University and Lamont-Doherty Earth Observatory, Palisades, NY, USA

10 ² Cooperative Institute for Research in Environmental Sciences (CIRES), University of Colorado, Boulder, CO, USA

³ Global Monitoring Laboratory, National Oceanic and Atmospheric Administration, Boulder, CO, USA

15 ⁴ Atlantic Oceanographic and Meteorological Laboratory, National Oceanic and Atmospheric Administration, 4301 Rickenbacker Causeway, Miami, FL, USA

Corresponding author: Amanda R. Fay afay@ldeo.columbia.edu

Key Points

- 20
- An updated surface water CO₂ climatology for 1980-2021 is created using the SOCAT database, following procedures of Takahashi et al. (2009)
 - A net air-sea CO₂ flux of -1.79 ± 0.7 PgC yr⁻¹ is determined for near-global ocean coverage

Abstract

25 The late Taro Takahashi (LDEO/Columbia University) and colleagues provided the first
near-global monthly air-sea CO₂ flux climatology in Takahashi et al. (1997), based on
available surface water partial pressure of CO₂ measurements. This product has been a
benchmark for uptake of CO₂ in the ocean. Several versions have been provided since,
with improvements in procedures and large increases in observations, culminating in
30 the authoritative assessment in Takahashi et al. (2009). Here we provide and document
the last iteration using a greatly increased dataset (SOCATv2022) and determining
fluxes using air-sea partial pressure differences as a climatological reference for the
period 1980-2021 (Fay et al. 2023). The resulting net flux for the open ocean region is
estimated as -1.79 ± 0.7 PgC yr⁻¹ which compares well with other global mean flux
35 estimates. While global flux results are consistent, differences in regional means and
seasonal amplitudes are discussed. Consistent with other studies, we find the largest
differences in the data-sparse southeast Pacific and Southern Ocean.

1. Introduction

40 As of the start of the 2020s, atmospheric carbon dioxide (CO₂) levels exceed 415 ppm
on an annual basis and the continued growth of the atmospheric reservoir represents a
major societal concern due to the impact on the radiative balance of the atmosphere.
Warming and associated environmental changes including sea-level rise and ocean
45 acidification have adverse effects on countless aspects of terrestrial and marine
ecosystems which in turn impact air-sea exchange of CO₂ and the trajectory of the
atmospheric CO₂ levels. The annually updated Global Carbon Budget (GCB) report
estimates current net global ocean carbon uptake has been estimated at nearly 3.0 PgC
per year, which corresponds to about a quarter of the total annual emissions (the total
50 anthropogenic CO₂ emission, including the cement carbonation sink, is estimated at
 10.9 ± 0.8 PgC yr⁻¹) (Friedlingstein et al. 2022). Given the importance of the ocean as a
CO₂ sink, it is essential to continuously monitor changes and improve our understanding
of the ocean's role in the global carbon cycle.

55 Over the last several decades, multiple approaches based on atmospheric and oceanic
observations have been developed to measure the impact of the ocean on the global
CO₂ cycle. These approaches include atmospheric inversions (Feng et al. 2019), global
atmospheric O₂/N₂ (Manning & Keeling 2006), ¹³C measurements (Quay et al. 1992,
Tans et al. 1993), ocean inventory approaches (Gruber et al. 2023) and the
60 measurement of surface ocean and atmospheric CO₂ (Takahashi et al. 1993). All

methods work towards the goal of elucidating the net flux of CO₂ from the atmosphere into the ocean. These different approaches have multiple advantages and disadvantages depending on the time and spatial scale of interest. Directly measuring surface ocean and atmospheric CO₂ levels has the advantage, given sufficient measurements, of deriving spatial and temporal variability over the ocean surface on short temporal and spatial scales. This method provides valuable insights into key processes driving the uptake and emissions of carbon when combined with our understanding of ocean physics and biological activity.

The surface ocean and atmospheric CO₂ approach leverages available observations and the dynamic sea-air gradient between the partial pressure of carbon dioxide (pCO₂) in the surface ocean (pCO₂^{oce}) and the overlying atmosphere (pCO₂^{atm}), known as the delta pCO₂ (ΔpCO₂) and typically defined as pCO₂^{oce} - pCO₂^{atm}. This difference is the thermodynamic driving force for the transfer of CO₂ into (negative) and out of (positive) the ocean. On average, the ΔpCO₂ across the global oceans are becoming increasingly negative as atmospheric CO₂ levels steadily rise, leading to an increasing carbon sink. Limited regions around the globe are sources of CO₂ to the atmosphere, including the equatorial Pacific Ocean and other areas of persistent upwelling.

The late Taro Takahashi was a leader in efforts to characterize air-sea CO₂ flux through the design and deployment of pCO₂ systems throughout the global oceans, and perhaps most importantly, his efforts to assemble, evaluate and construct global ocean climatologies from available pCO₂^{oce} datasets. Building on early collaborative work looking at ocean sources and sinks of carbon (Tans et al. 1990), many versions of the ocean pCO₂ climatology have been presented in literature (Takahashi et al. 1997, 2002, 2009a,b, and 2014), henceforth referred to as T-1997, T-2002, T-2009, and T-2014. The climatologies have been highly utilized and cited by carbon cycle researchers from around the world and form a basis for current advancements in quantifying the ocean carbon sink.

Here, we present an updated near-global climatological mean distribution and net sea-air CO₂ flux which represent the mean of ocean conditions over the last four decades. This climatology is unique compared to other advanced machine learning approaches (e.g., Rödenbeck et al. 2015) in that it interpolates in time and space using only the available pCO₂ data rather than using proxy variables for gap filling. This difference in methodology provides a valuable alternative approach to the ongoing effort to characterize the global ocean carbon sink. This benchmark is critical for global carbon assessments, notably the Regional Carbon Cycle Assessment and Processes (RECCAP2, DeVries et al. 2023) effort.

100

Building on previous work of Takahashi and colleagues, we employ the same time-space interpolation method used in the previous versions of the Takahashi climatology (e.g., T-2002, T-2009, T-2014) to create the climatology. However, here we use the Surface Ocean CO₂ Atlas (SOCAT) v2022 database (Bakker et al. 2016, 2022), rather than the LDEO database curated by Taro Takahashi. We use the SOCAT database for this update because it is the most comprehensive database of available observations from international research groups. We have included the climatology produced using the most recent LDEO database (LDEOv2019, Takahashi et al. 2020) with data extending to 2019, in supplementary figures and text but our main findings will focus on the results from the SOCAT database.

2. Data

2.1 SOCAT database

The SOCAT database was first released in 2011 (Pfeil et al. 2013) and is updated annually (Bakker et al. 2016). Observations are reported as values of fugacity of CO₂ (fCO₂) in micro atmospheres (μatm), along with a collection of ancillary data including concurrent observations such as SST (more accurately, the ship intake temperature), temperature of equilibration, salinity, and sea level pressure at the time of equilibration. The SOCAT database also includes supplemental variables with values interpolated from gridded global datasets such as satellite SST and NCEP sea level pressure. The database restricts the included data to only observations that are measured in near-continuous operation or in discrete samples with an equilibrator system. This means that it does not include fCO₂ values that are calculated from other ocean carbon measurements including dissolved inorganic carbon, total alkalinity and/or pH. For this analysis we select SOCAT data from cruises with flags A-D and observations with a World Ocean Circulation Experiment (WOCE) flag of 2 (Pfeil et al. 2013). More information on the SOCAT database is available in Bakker et al. (2016); current and previous releases are available to download at <https://www.socat.info/index.php/data-access/>.

The SOCAT database (Bakker et al. 2016) is the largest and most widely used collection of quality-controlled fCO₂ data with over twice the number of observations included in the latest LDEO database (LDEOv2019). In this work, we utilize the SOCATv2022 release which includes over 33.7 million observations spanning the years 1957 through 2021 (DOI:10.25921/1h9f-nb73, accessed on July 15, 2022, Bakker et al., 2022). We use observations beginning in 1980 due to limited metadata available for earlier observations. This time restriction eliminates only 24,786 observations, or less

140 than 0.1% of the total number of observations included in the SOCATv2022 release. We also exclude coastal observations collected within 100km of land similar to past LDEO climatologies which reduces the total number observations utilized to just over 21.3 million. Unlike past LDEO climatologies, this climatology does not exclude observations collected in the equatorial Pacific during El Niño periods.

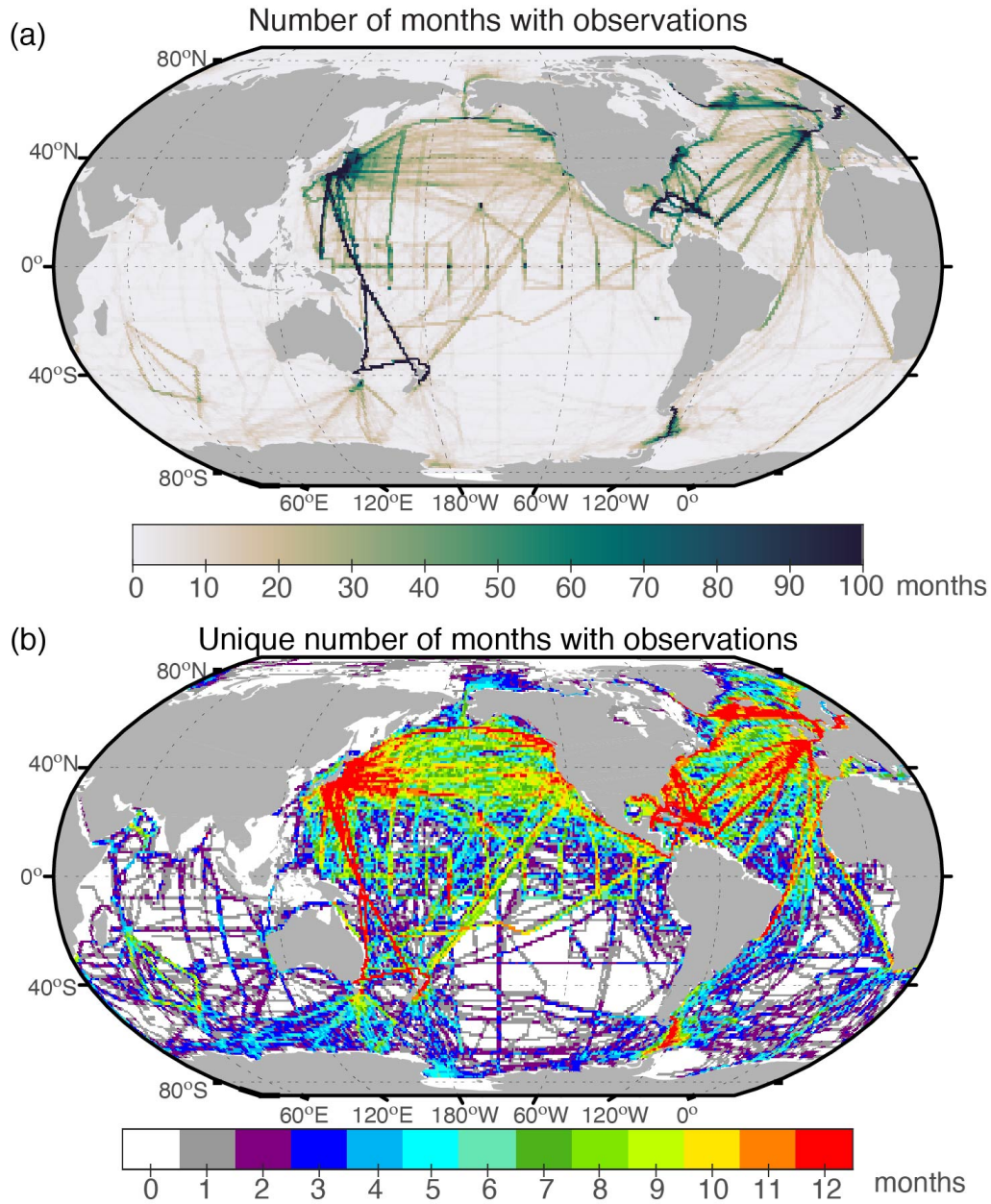
2.2 $f\text{CO}_2$ vs $p\text{CO}_2$

145 For this climatology, we report values of the fugacity of carbon dioxide ($f\text{CO}_2$) rather than $p\text{CO}_2$. The $f\text{CO}_2$ is equal to the $p\text{CO}_2$ corrected for non-ideality of CO_2 solubility in water using the virial equation of state (Weiss 1974). The fugacity correction for surface water is 0.996 and 0.997 at 0 °C and 30 °C respectively (Dickson et al. 2007), or 0.7 to 1.2 μatm lower than the corresponding $p\text{CO}_2$, and depends primarily on temperature for the conversion although pressure is also included in the conversion equation. It is now
150 common practice in the observational community to present observed values as $f\text{CO}_2$ and this option has been endorsed by the IOCCP (International Ocean Carbon Coordination Project). The correction of $p\text{CO}_2^{\text{oce}}$ and corresponding $p\text{CO}_2^{\text{atm}}$ values to $f\text{CO}_2$ is practically identical such that the resulting $\Delta f\text{CO}_2$ is always within 0.1 μatm compared to the corresponding $\Delta p\text{CO}_2$. As a result, this difference will not have a
155 meaningful impact on air-sea flux calculations. Only at elevated $f\text{CO}_2$ levels, such as those in the subsurface ocean, is the difference between $f\text{CO}_2$ and $p\text{CO}_2$ significant. Therefore, the shift in this climatology from $p\text{CO}_2$ to $f\text{CO}_2$ simply aligns this updated climatology with current community best practices. This choice avoids conversions given that the SOCAT database reports $f\text{CO}_2$ values.

160

2.3 Distribution of measurements

At present, the SOCAT database relies on voluntary submission of quality-controlled data from over 100 scientists. The number of observations has increased significantly over past decades, facilitated by a now-automated data submission process. Even with
165 this increase in observations, there are only a few regions over the global oceans where $f\text{CO}_2^{\text{oce}}$ has been systematically monitored over multiple decades at nearly the same location (Bakker et al. 2016; Bates et al. 2014; Landschützer et al. 2016, Figure 1). Of the observations considered in this analysis, spanning years 1980-2021, only 1.4% of the monthly 1° by 1° global ocean grid cells have measured values. Most of the data
170 (65%) was collected since 2010.



175 Figure 1: (a) Total number of months with at least one observation in each 1° grid cell in the SOCATv2022 database, for years 1980-2021 (Bakker et al. 2022). The maximum number possible for a grid cell is 504 (42 years * 12 months). (b) the number of unique calendar months in each grid cell where at least one observation has been made since 1980. Red indicates grid cells where each month (Jan - Dec) has been sampled at least once over the 40+ year time series while white indicates grid cells with no measurements over the length of the time series.

180

185 An additional challenge to global monitoring efforts is that observations are not collected consistently throughout the annual cycle in many locations around the globe, thus requiring considerable interpolation to produce a full seasonal climatology. Much of the ocean contains data collected in fewer than three unique months of the year, regardless of how many years of data is available (Figure 1b). Current efforts utilize proxy variables and machine learning to identify relationships between ocean carbon and better-
190 observed variables (often SST, chlorophyll, mixed layer depth, etc.) and then through those relationships extrapolate available ocean $f\text{CO}_2$ to fill the missing months of the seasonal cycle. Unlike those methods (e.g., methods compared by Rödenbeck et al. 2015), we do not utilize any proxy variables in this method and only rely on available $f\text{CO}_2^{\text{oce}}$ values in the SOCAT database to estimate the seasonal climatology. Hence,
195 this effort provides a complementary alternative interpolation method to other approaches.

2.4 Atmospheric $f\text{CO}_2$

For the calculation of atmospheric carbon dioxide, we utilize zonally invariant NOAA
200 marine boundary layer (MBL) $x\text{CO}_2$ values which are reported in units of ppm or $\mu\text{mol/mol}$ (Lan et al. 2023) and provided with each observation in the SOCAT dataset. In order to calculate $f\text{CO}_2^{\text{atm}}$ values from MBL $x\text{CO}_2^{\text{atm}}$ values, we follow standard operating procedures and equations outlined in Dickson et al. (2007) and use the SST, salinity and sea level pressure observations also reported for each value in the SOCAT
205 database (Bakker et al. 2022). The SST (more specifically, ship intake temperature) is measured concurrently with surface ocean CO_2 , sea level pressure is from the National Centers for Environmental Prediction (NCEP), and surface salinity is from the World Ocean Atlas (WOA). Delta $f\text{CO}_2$ ($\Delta f\text{CO}_2$) is calculated by subtracting corresponding atmospheric from ocean values ($f\text{CO}_2^{\text{oce}} - f\text{CO}_2^{\text{atm}}$).

210

3. Methods

3.1 Normalization to a reference year

In previous versions of the LDEO climatology, emphasis was placed on the calculation
215 of trends in surface ocean carbon levels for all regions of the global ocean. These trends were used to normalize all available observations to one reference year by correcting for the estimated change that would be expected between the collection date of the observation and the reference year. In this updated climatology, we use $\Delta f\text{CO}_2$

220 values as input to the algorithm rather than allowing for the adjustment of $f\text{CO}_2^{\text{oce}}$ to a specific reference year. A similar methodology was used in early versions of the LDEO climatology (i.e., T-1997).

225 By utilizing this method to collapse all available data to one year, we make the assumption (as made by T-1997) that the ocean and atmosphere are changing at the same rate and thus the $\Delta f\text{CO}_2$ has been constant over the 40+ years of observations. This assumption allows for a standard method for the normalization of all observations to one calendar year. This method is utilized in contrast to the most recent LDEO climatologies where trends over distinct time periods were investigated and one trend then selected for use in time-normalization throughout much of the global ocean (i.e., T-2002, T-2009, and T-2014).

235 Atmospheric $p\text{CO}_2$ change drives rising ocean $p\text{CO}_2$, and surface ocean carbon concentrations follow atmospheric increases on multi-decadal timescales and over large regions and the global scale (Fay & McKinley 2013, McKinley et al. 2020). Large synthesis efforts by those in the global ocean carbon community show that even if ocean trends are larger/smaller than the atmosphere on decadal or multi-year time periods, when considering the longest time periods, the atmosphere and ocean carbon trends are statistically indistinguishable over much of the global ocean (Fay & McKinley 2013, Tjiputra et al. 2014). While the Tjiputra et al (2014) and Fay & McKinley (2013) efforts consider large regional analysis, Bates et al. (2014) provides a synthesis of trends in $p\text{CO}_2$ at long-term observing stations, with most of the stations showing a match to the rise in atmospheric CO_2 concentration (Tanhua et al. 2015).

245 Supplementary Table 1 shows biome-scale mean $f\text{CO}_2$ trends computed using all available $1^\circ \times 1^\circ$ grid cells with observations in the gridded product released as part of SOCATv2022 (Sabine et al. 2013). We present seasonal trends for each biome due to seasonal sampling bias over much of the global oceans. Similar to T-2009 (see Tables 1-5 of T-2009), trends for different ocean regions vary significantly (Supplementary Table 1) due in part to differing years with available data across ocean regions (Supplementary Figure 5). Observations within the Indian Ocean, for example, and other regions with blue shading in Supplementary Figure 5 are weighted towards the 1980's and 1990's while regions stretching across the North Atlantic and North Pacific have been heavily sampled over the last two decades with ships of opportunity. These well sampled regions have median years of collected observations later than 2010 (areas with red shading in Supplementary Figure 5).

255 Recent studies (Friedlingstein et al. 2022) demonstrate that globally, the oceans lag slightly behind the atmosphere in terms of rates of carbon increase, and thus $\Delta f\text{CO}_2$ has

260 become increasingly negative as noted above. The central climatological year
represented by our method is thus somewhat ambiguous regionally, though globally it is
centered at about 2010. The median year of all fCO₂ observations collected in
SOCATv2022 greater than 100km from land is 2013. Since observations are more
densely clustered in the recent period, observations in the early period may have a
greater weight in determining climatological values. Given global trends, our approach
265 may estimate a smaller ocean sink in regions where the ocean was sampled more
heavily early in the time period (e.g., blue shading in Supplementary Figure 5) and a
greater ocean sink in regions with heavy recent sampling (red shading in
Supplementary Figure 5). We acknowledge that the assumption of a constant $\Delta f\text{CO}_2$
does not take into account the long-term trend in $\Delta f\text{CO}_2$, however, our simplified
270 approach avoids application of trends determined for well-observed regions and time
periods across poorly-observed regions and time periods.

We conducted a sensitivity analysis to demonstrate the impact of the $\Delta f\text{CO}_2$ method
implemented in this version versus a normalization approach similar to that applied in T-
275 2009. Specifically, we assumed a homogeneous $1.5 \mu\text{atm yr}^{-1}$ trend in fCO₂^{oce} for all
regions and years, and normalized available observations to a reference year of 2010.
Spatial maps of the differences in fCO₂ for the year 2010 for the normalization approach
versus $\Delta f\text{CO}_2$ method are shown in the supplemental information (Supplementary
Figure 6). Globally, the annual ocean uptake created using the $1.5 \mu\text{atm yr}^{-1}$
280 normalization method (T-2009) is within 3% of the $\Delta f\text{CO}_2$ method (this analysis)-
specifically, $-1.85 \text{ PgC yr}^{-1}$ versus $-1.79 \text{ PgC yr}^{-1}$ for the $1.5 \mu\text{atm yr}^{-1}$ normalization
method and the presented $\Delta f\text{CO}_2$ approach, respectively, for a reference year of 2010.

3.2 Method for time–space interpolation

285 The method for spatial interpolation and day of year utilized in the climatology has not
changed from the previous versions (e.g., T-2009). As described above, $\Delta f\text{CO}_2$ values
are used to compile observations into one reference year in contrast to the time-
normalization approach of T-2009. The spatial interpolation scheme requires that all
observations are binned into $4^\circ \times 5^\circ$ grids for each day of the year. In some areas of the
290 global ocean, such as the northern and equatorial ocean regions, there are
observations in a majority of the pixels. However, vast expanses in the Southern
Hemisphere have few observations in each pixel and there are many pixels that contain
no observations at all (Figure 1).

295 We follow the same methodology as T-2009 for binning observations in sparsely
sampled grid cells south of 12°S . Here, spatial binning is increased by 4° and 5°
longitude and latitude, respectively, extending from the center of each grid cell. This

creates a grid of overlapping $8^{\circ} \times 10^{\circ}$ grid cells. Additionally, bins include the day before and after a given day of year. The mean is computed by weighting measured values
300 inversely proportional to their time-space distance from the pixel center. After the above procedures are applied, more than 50% of the space–time pixels over the global oceans are filled.

To estimate the $\Delta f\text{CO}_2$ values in the remaining cells, an interpolation equation based on
305 the 2-D diffusion–advection transport of surface waters is used, as in T-2009. The equation is discretized onto a $4^{\circ} \times 5^{\circ}$ grid for the global ocean, and solved iteratively using a finite difference algorithm (Takahashi et al. 1995, T-1997). The method avoids singularities at the poles by assigning land to each high latitude region (Antarctica in the south and treating the highest latitudes of the Arctic Ocean as land in the north). With
310 this method, the resulting $\Delta f\text{CO}_2$ values are the solutions obtained after 500 iterations, as previously determined on the basis of interpolation experiments of temperature values (T-2009).

With this interpolation scheme, observed $\Delta f\text{CO}_2$ values where available are preserved,
315 and the continuity equation is used to compute values for grid cells that have no observations. Consistent with previous iterations of this approach, the combined effects of internal sources and sinks of carbon, CO_2 exchange with the atmosphere, as well as upwelling of deep waters are all assumed to be included in the analysis of the observations that feed into the interpolation scheme. Uncertainties persist due to the
320 sparsity of input data, normalization to a reference year, and the space-time interpolation. In part to address these uncertainties, we report only monthly means.

To maintain consistency with similar products and input datasets for flux calculations, we downscale to one-degree boxes by assigning all 20 $1^{\circ} \times 1^{\circ}$ pixels in a $4^{\circ} \times 5^{\circ}$ grid cell
325 the same $\Delta f\text{CO}_2$ value. When calculating sea-air fluxes, because the other inputs to the flux calculation such as wind speed, are varying on a $1^{\circ} \times 1^{\circ}$ degree resolution grid, differences in the gridded flux climatology emerge on this finer spatial scale.

3.3 Flux calculation method: pySeaFlux

330 To assess the near-global ocean carbon sink associated with these $\Delta f\text{CO}_2$ estimates, air-sea CO_2 exchange must be calculated. The gridded monthly $1^{\circ} \times 1^{\circ}$ $\Delta f\text{CO}_2$ values were used to compute air-sea CO_2 fluxes using the bulk formulation with python package Seaflux.1.3.1 (<https://github.com/lukegre/SeaFlux>, Gregor & Fay, 2021). The net sea–air CO_2 flux (F) is estimated using:

335
$$\text{Flux} = kw \cdot \text{sol} \cdot (f\text{CO}_2^{\text{oce}} - f\text{CO}_2^{\text{atm}}) \cdot (1 - \text{ice}) \quad \text{Eq. (1)}$$

where k_w is the gas transfer velocity, sol is the solubility of CO_2 in seawater (in units of $mol\ m^{-3}\ \mu atm^{-1}$), fCO_2^{oce} is the partial pressure carbon in the surface ocean (in μatm), and fCO_2^{atm} (in units of μatm) represents the atmospheric CO_2 levels in the marine boundary layer. Finally, to account for the seasonal ice cover at high latitudes, the fluxes are weighted by one minus the ice fraction (ice), i.e., the open ocean fraction. By utilizing the pySeaFlux package (Fay & Gregor et al. 2021, Gregor & Fay 2021), we are able to include multiple scaled gas transfer velocities for three different wind products and our resulting flux estimate is a mean of the three. Additional inputs to the flux calculation include EN4.2.2 salinity (Good et al. 2013), SST and ice fraction from NOAA Optimum Interpolation Sea Surface Temperature V2 (OISSTv2, Reynolds et al., 2002), European Centre for Medium-Range Weather Forecasts (ECMWF) ERA5 sea level pressure (Hersbach et al. 2020). Finally, surface winds and associated wind scaling factor for the Cross-Calibrated Multi-Platform v2 (CCMP2; Atlas et al. 2011), the Japanese 55-year Reanalysis (JRA- 55; Kobayashi et al. 2015), and the ECMWF ERA5 (Hersbach et al. 2020) reanalysis products are used.

Fluxes reported here use inputs from the year 2010 for the k_w , sol , and ice fraction variables. Alternatively, we have calculated fluxes using a mean over a 17-year time period centered on the year 2010. This yields a very similar value with the mean difference being a $0.04\ PgC\ yr^{-1}$ increase in estimated carbon uptake.

4. Results

4.1 Climatological mean distribution of surface water ΔfCO_2

4.1.1 Global

The near-global 12-month climatological mean distribution of ΔfCO_2 (fCO_2^{oce} minus fCO_2^{air}) is reported for the SOCAT database (Figure 2, Fay et al. 2023). Evident in the mapped climatology are the large-scale patterns across the global ocean: the consistent high (positive) ΔfCO_2 values in the equatorial Pacific region where upwelling is a dominant influence, and low (negative) values of ΔfCO_2 in the North Atlantic region where evaporation leads to increase salinity and cooling driving strong uptake of carbon and subduction of surface waters.

A near-global mean climatology curve shows a bimodal shape in ΔfCO_2 , with a smaller peak in boreal spring (March/April) and a much larger peak in late boreal summer (August/September), clearly driven by the hemispheric seasonal cycles (Figure 2a). The global curve reaches its minimum in November and begins a recovery throughout the

boreal winter before dipping again to a springtime minimum in June. The near-global
 375 annual mean $\Delta f\text{CO}_2$ value is $-4.1 \mu\text{atm}$ (with temporal standard deviation equal to 1.6
 μatm) and it is notable that the global mean $\Delta f\text{CO}_2$ value is below zero for every month
 of the year, suggesting that seasonally the global ocean mean is a perpetual carbon
 sink with expansive regions of uptake nearly always outweighing smaller regions of
 efflux (Figure 2, 3). On the other hand, the northern and southern hemispheric seasonal
 380 cycles each exhibit peaks in $\Delta f\text{CO}_2$ above zero during their corresponding
 warm/summer months (Figure 2a).

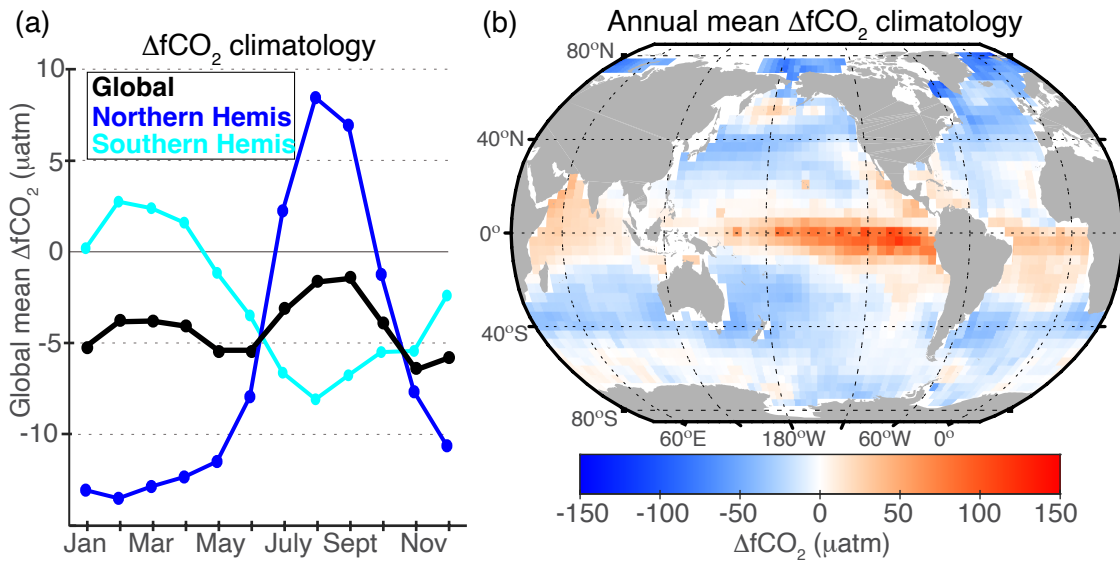


Figure 2: (a) Global mean and Northern and Southern Hemisphere $\Delta f\text{CO}_2$ seasonal climatology from the SOCAT database. (b) Map of annual $\Delta f\text{CO}_2$ climatology.

385

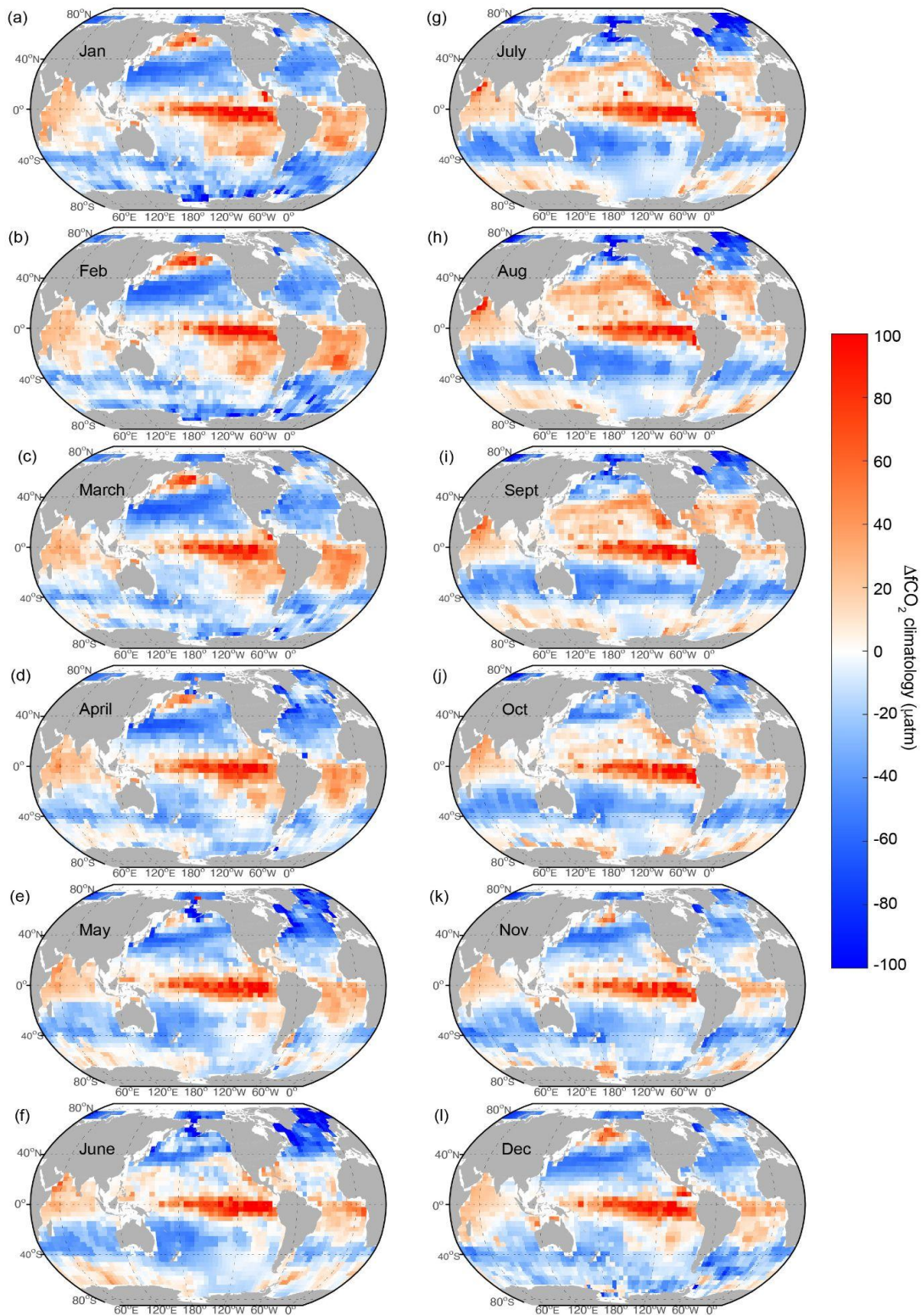
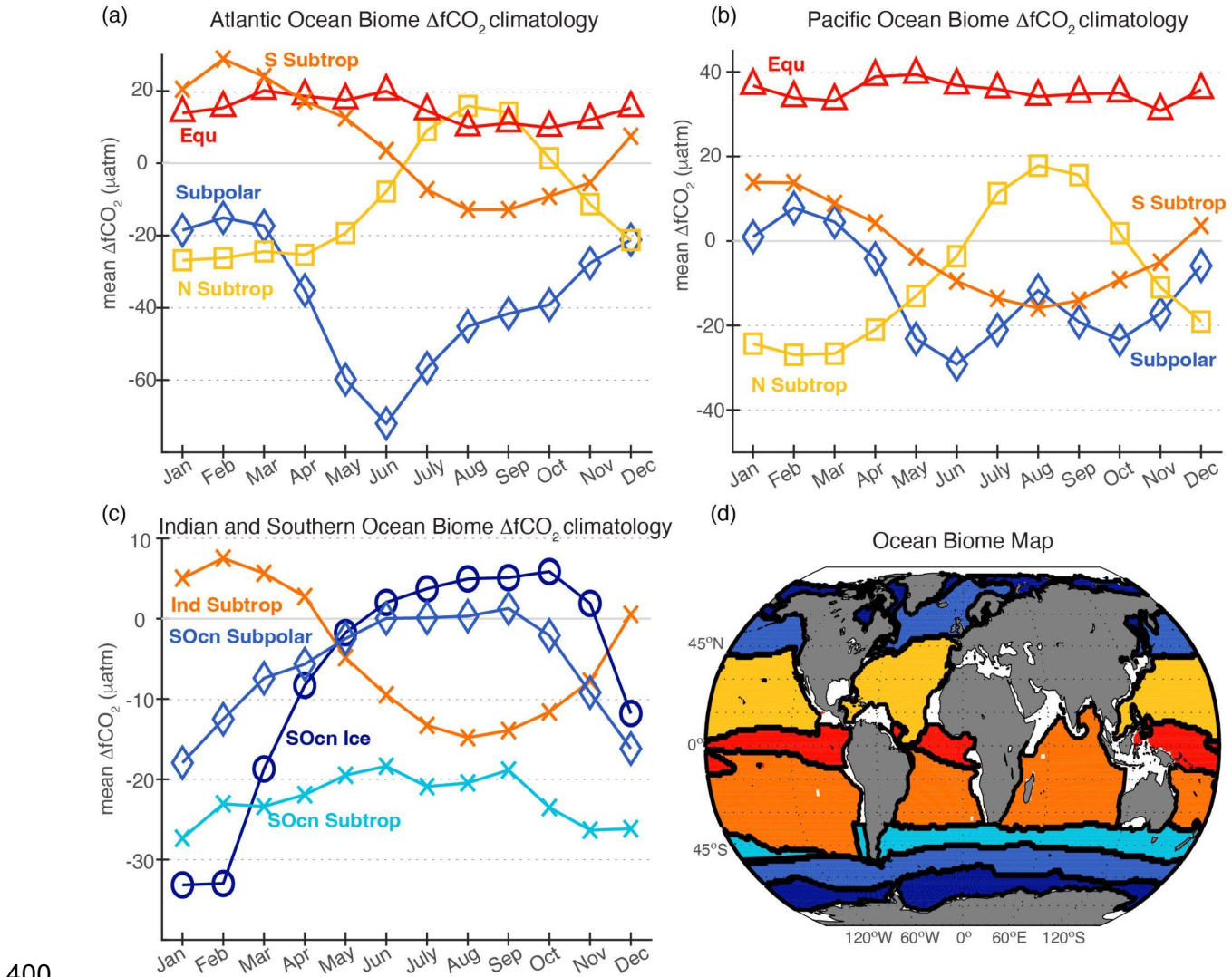


Figure 3: Monthly mean values for sea–air $\Delta f\text{CO}_2$. Warm colors indicate positive $\Delta f\text{CO}_2$ (ocean is greater than atmospheric CO_2), white indicates near zero $\Delta f\text{CO}_2$, and cool colors indicate negative $\Delta f\text{CO}_2$ (ocean CO_2 is lower than the atmosphere).

390 4.1.2 Regional

To show the seasonal changes in ΔfCO_2 more clearly it is valuable to consider the patterns exhibited over consistent biogeochemical regions around the globe. For this analysis we utilize the biomes of Fay & McKinley (2014), but for simplicity we combine the seasonally stratified and permanently stratified subtropical biomes into one region in the Northern Hemisphere (referred to simply as subtropical in this manuscript). Monthly climatologies for each of the biomes are shown (Figure 4) in addition to the gridscale maps for each climatological month which allows for further regional interpretation (Figure 3). Table 1 lists the annual mean ΔfCO_2 values in each of these regions.



400 Figure 4: Monthly climatology of ΔfCO_2 for each regional ocean biome in the (a) Atlantic, (b) Pacific, (c) Indian and Southern Ocean basins. (d) Map of regional biomes. Colors of curves correspond to regions on the map in (d) with labels in matching colored text.

405 Note that the y-axis varies between subplots. Values for each region's annual mean and standard deviations listed in Table 1.

410 The equatorial regions of the Pacific and Atlantic oceans have positive $\Delta f\text{CO}_2$ values throughout the annual cycle and little seasonal variability. This indicates that the area is a source of CO_2 to the atmosphere year round. The equatorial Pacific (Figure 4b) has the highest positive $\Delta f\text{CO}_2$ values (annual mean = $35.4 \mu\text{atm}$), followed by the tropical Atlantic (Figure 4a, annual mean = $14.8 \mu\text{atm}$).

415 The subtropical biomes, representing the temperate North and South Atlantic and Pacific basins exhibit large seasonal $\Delta f\text{CO}_2$ cycles which change sign throughout the year. Here, the $\Delta f\text{CO}_2$ cycle is largely temperature driven. Positive $\Delta f\text{CO}_2$ in warm summer months and negative values in colder winter months reflecting the dominance of seasonal temperature changes on the cycles of ocean $f\text{CO}_2$ in these regions. The seasonal amplitude for the subtropical North Pacific is $44.7 \mu\text{atm}$, and is slightly larger than the seasonal amplitude in the subtropical North Atlantic ($42.7 \mu\text{atm}$). Since the mean seasonal amplitudes for SST are quite similar in these two ocean basins, with the Atlantic having a slightly larger seasonal change in surface temperature (4.4°C in Pacific and 5.0°C in Atlantic, not shown), the difference in $\Delta f\text{CO}_2$ amplitudes between the Pacific and Atlantic subtropical regions cannot be attributed solely to SST, and may reflect differences in biogeochemical cycling between these two basins.

430 Seasonal changes in the northern subtropical oceans are roughly six months out of phase from the southern subtropical biomes. The South Pacific subtropical biome has a seasonal amplitude of $29.8 \mu\text{atm}$ which is nearly $15 \mu\text{atm}$ smaller than that of the North Pacific subtropical biome. In contrast, the seasonal amplitude of the South Atlantic subtropical basin is just $1 \mu\text{atm}$ smaller than its counterpart in the North Atlantic (the South Atlantic subtropical amplitude is $41.7 \mu\text{atm}$). The Indian Ocean subtropical biome which encompasses most of the Indian Ocean, both above and below the Equator, has a smaller $\Delta f\text{CO}_2$ amplitude ($22.3 \mu\text{atm}$), but the phasing matches well with both the South Pacific and South Atlantic subtropical biomes, with peak (positive) $\Delta f\text{CO}_2$ values in February and the lowest values in August. The smaller $\Delta f\text{CO}_2$ seasonal amplitudes in the Indian and South Pacific subtropical basins are partially attributable to lower SST variability in these regions (SST seasonal cycle amplitudes are 4.0°C and 3.0°C in the South Pacific and Indian subtropics, respectively, compared to 4.6°C in the subtropical South Atlantic). However, it is likely that both differences in spatiotemporal patterns of primary productivity and undersampling in the South Pacific and Indian subtropics (Figure 1) also contribute to differences in $\Delta f\text{CO}_2$ seasonal amplitudes between these basins.

445 The timing of the $\Delta f\text{CO}_2$ trough in the subpolar regions is opposite that of the subtropical
 North Pacific and Atlantic basins. Strongly negative $\Delta f\text{CO}_2$ in the spring and summer
 months is due to the effects of intense biological drawdown which quickly and
 dramatically lowers carbon levels in the subpolar surface ocean with the onset of the
 450 subpolar seasonal cycles that are roughly four to six months out of phase compared to
 adjacent subtropical regions. In the Atlantic subpolar biome, $\Delta f\text{CO}_2$ values are
 consistently below zero throughout the annual cycle (a maximum of $-15.1 \mu\text{atm}$ occurs
 in February). In the subpolar North Pacific basin, positive $\Delta f\text{CO}_2$ values are present over
 the boreal winter (Jan-March) before biological drawdown associated with the spring
 455 bloom lowers the $\Delta f\text{CO}_2$ values back below zero for the remainder of the year. The
 spring drawdown is weaker in the subpolar North Pacific compared to the subpolar
 North Atlantic.

Figure 4c displays the seasonal cycle for the Southern Ocean biomes including the
 460 seasonal ice biome, the subpolar region, and the seasonally stratified subtropical region
 of the Southern Hemisphere. The higher latitude subtropical region has negative $\Delta f\text{CO}_2$
 values throughout the year and a relatively small seasonal $\Delta f\text{CO}_2$ amplitude compared
 to the more expansive South Atlantic, South Pacific and Indian subtropical basins to the
 north. The mean $\Delta f\text{CO}_2$ and seasonal amplitude for the Southern Ocean subtropical
 465 region is $-22.5 \mu\text{atm}$ and $9.0 \mu\text{atm}$, respectively.

The Southern Ocean subpolar and ice biomes both have relatively strong seasonal
 cycles, reaching maximums of $\Delta f\text{CO}_2$ near and slightly above zero, respectively, during
 the late austral winter and early austral spring (Figure 4c). This positive peak during July
 470 through October in the Southern Ocean seasonal ice zone is influenced by under-ice
 vertical mixing with deep waters that contain excess carbon and nutrients. During the
 austral spring and summer months, intense phytoplankton blooms occur near and
 around the edges of the retreating sea ice in the seasonal ice zone and within the
 subpolar region. These blooms cause dramatic drops in $\Delta f\text{CO}_2$ values at the end of the
 475 calendar year (Oct-Dec). Limited sampling and smoothing from the interpolation method
 fail to capture the high spatiotemporal variability that characterizes this highly dynamic
 region.

Biome	$\Delta f\text{CO}_2$ (μatm)	Flux (PgC yr^{-1})	Area (10^6 km^2)
NP Ice	-24.6 (9)	-0.02 (0.02)	4.2
NP SPSS	-11.5 (12)	-0.11 (0.11)	12.8
NP Subtropics	-8.2 (16)	-0.40 (0.53)	47.9

Pacific Equ	35 (2)	0.35 (0.03)	26.4
SP Subtropics	-2.3 (10)	-0.14 (0.31)	52.7
NA Ice	-19.3 (4)	-0.04 (0.01)	4.5
NA SPSS	-36.2 (17)	-0.27 (0.08)	9.7
NA Subtropics	-10.0 (16)	-0.24 (0.26)	23.4
Atlantic Equ	14.7 (3)	0.04 (0.01)	7.4
SA Subtropics	5.6 (14)	0.01 (0.12)	18.1
Indian Subtropics	-4.5 (8)	-0.18 (0.16)	35.9
SO STSS	-22.1 (3)	-0.59 (0.06)	29.6
SO SPSS	-6.0 (6)	-0.21 (0.22)	30.7
SO Ice	-6.8 (14)	-0.08 (0.12)	18.7

480 Table 1. Mean annual DfCO₂ and flux in global open ocean biomes (Fay & McKinley
 2014). Value in parentheses is one standard deviation over the 12-month climatology.
 Area of each biome also included. NP: North Pacific; SP: South Pacific; NA: North
 Atlantic; SA: South Atlantic; SO: Southern Ocean. SPSS: Subpolar seasonally stratified;
 STSS: Subtropical seasonally stratified. Northern hemisphere subtropical regions are
 485 reported to match the regions shown in Figure X (combining the STPS and STSS
 biomes from Fay & McKinley 2014 into one).

4.2 Net air-sea CO₂ flux

490 The mean climatological global air-sea CO₂ flux estimate using the SOCAT database is
 -1.79 PgC yr⁻¹, indicating uptake of carbon by the ocean. This is a slightly greater flux
 into the ocean than the direct estimate from the previous version of the climatology (T-
 2009), which reported a direct estimated global mean flux of -1.4 PgC yr⁻¹ for the year
 2000. For the uncertainty in global ocean-atmosphere CO₂ flux, we use the methods
 495 described in T-2009 with updated uncertainty estimates as reported when applicable.
 Wanninkhof et al. (2013) followed the same approach as T-2009 with consideration of
 updated synthesis work (Ho et al. 2011). Our approach combines uncertainty
 contributions from the spatial (13% or ±0.23 (T-2009)) and temporal (±0.5 PgC yr⁻¹ (T-
 2009)) sampling of ΔfCO₂ as well as smaller contributions for the uncertainty in the gas
 500 exchange parameterization (20% or ±0.36 PgC yr⁻¹, Wanninkhof 2014), wind (±0.09
 PgC yr⁻¹ (Fay & Gregor et al. 2021) and riverine carbon (±0.2 PgC yr⁻¹, Jacobson et al.,
 2007). This yields an uncertainty estimate of ±0.7 PgC yr⁻¹ (when summed in
 quadrature) on our mean climatological global air-sea CO₂ flux estimate.

505 Results discussing the net flux produced from the LDEO pCO₂ database climatology is
 included in the supplementary material.

4.2.1 Mean annual distribution

The near-global mean flux estimate presented here represents 90% of the surface area of the global ocean. Specifically, this estimate excludes the coastal ocean and areas of the high latitude seas. We have chosen to present the near-global flux value discussed above without any adjustment to which could account for missing areas. Suggested methods for filling missing ocean areas in such reconstructions are available in Fay & Gregor et al. (2021) but are not implemented in this climatology to remain consistent with its previous versions. An estimate of the flux from regions missing from this product can be obtained by using the full-coverage pCO₂ climatology combining open and coastal oceans (Landschützer et al. 2020). Considering only grid cells in the Landschützer et al. (2020) product that are missing in this climatology, we estimate an annual average coastal and high latitude flux of -0.38 PgC yr⁻¹. The flux adjustment for missing areas of this climatology varies throughout the seasonal cycle, ranging from -0.43 to -0.31 PgC yr⁻¹ during the 12 months of the climatology. This quantity is not included in the climatological estimate presented here.

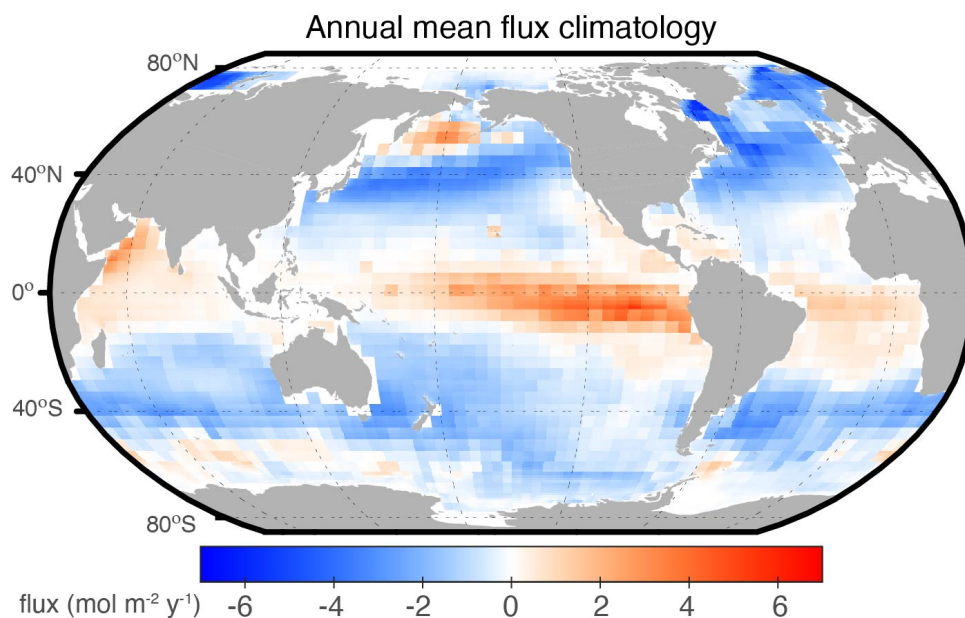


Figure 5: Annual mean CO₂ flux calculated from the SOCAT database. Flux is calculated using the SeaFlux method using the mean of three wind speed reanalysis products. Warm and cool colors indicate regions of carbon efflux and uptake, respectively. The near-global mean flux is -1.79 PgC yr⁻¹.

Figure 5 shows the climatological mean annual sea-air CO₂ flux (mol m⁻² yr⁻¹) and maps of two seasons (DJF and JJA) are displayed in Figure 6. Annual mean sea-air CO₂ flux values for the ocean regions are summarized in Table 1. The equatorial Pacific is the

most prominent atmospheric CO₂ source region, with a seasonally persistent sea-to-air flux of 0.35 PgC yr⁻¹. When combined with the equatorial Atlantic region, the tropical belt
535 emits an annual mean of 0.39 PgC yr⁻¹ to the atmosphere. Adjacent to this tropical efflux zone, are vast expanses of seasonally-variable flux patterns. The subtropical basins in both hemispheres act as CO₂ sinks in the cooler months and transition to regions of neutral or small CO₂ sources during the warmer months. At higher subtropical latitudes, strong winds and relatively low ocean fCO₂ occur along the subtropical
540 convergence zone where the cooled subtropical gyre waters with low fCO₂ meet the subpolar waters with biologically-lowered fCO₂.

The Northern Hemisphere mid and high latitude regions represent a smaller sink compared to the corresponding regions of the Southern Hemisphere (Table 1) largely
545 due to the overall greater surface area of the oceans in the Southern Hemisphere (oceans south of 35S are 25% of total global ocean area while oceans north of 35N are 15% of total ocean area). The dramatic influence of the expansive Southern Hemisphere oceans is also demonstrated by the large flux in the Southern Ocean subtropical region (-0.59 PgC yr⁻¹) that represents 8% of the global ocean surface area.

550 Moving poleward, a strong sink (-0.27 PgC yr⁻¹) occurs in the North Atlantic subpolar region which includes the Nordic Seas and the portions of the Arctic Ocean which contain observations. This strong localized carbon sink is attributed to the import of low anthropogenic waters at depth in the Gulf Stream that are exposed as mixed layers
555 deepen (Ridge & McKinley 2020), and large phytoplankton blooms in spring followed by cooling in winter. In the Southern Ocean, annual mean CO₂ flux is heterogeneous and relatively small in the seasonal ice zone due to the ice cover that reduces sea-air gas transfer in winter. Additionally, the small annual flux values in the Southern Ocean subpolar and ice regions (-0.21 PgC yr⁻¹ and -0.08 PgC yr⁻¹, respectively) are a result of
560 a cancellation of the seasonal source (winter) and sink (summer) fluxes.

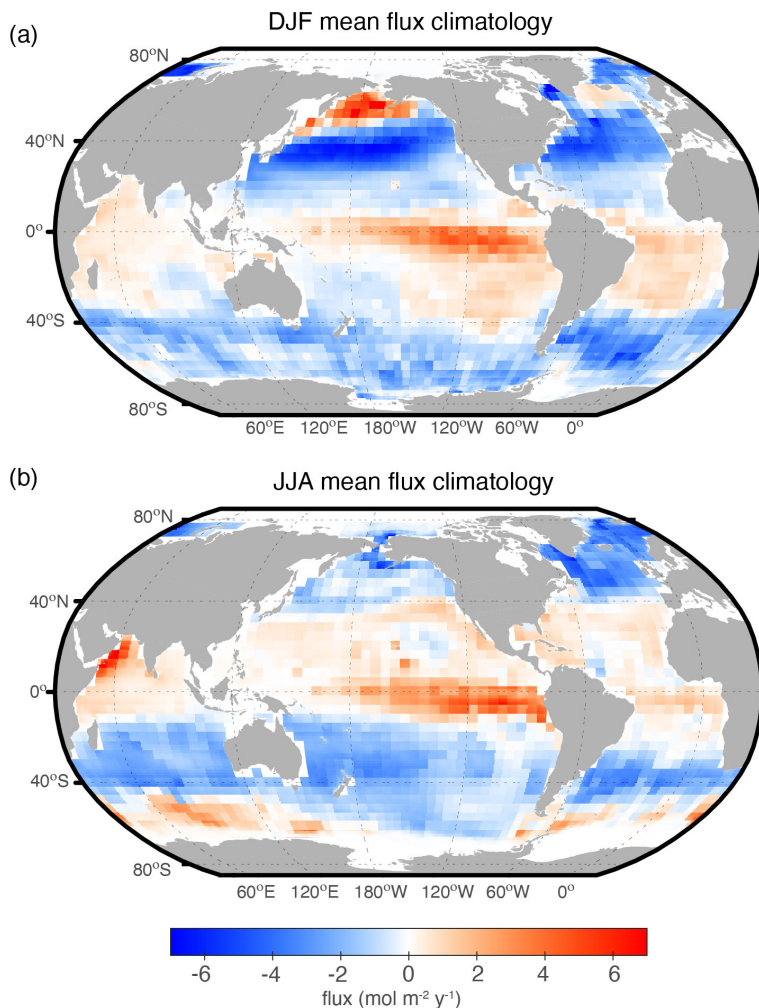
4.2.2 Seasonal variation of sea-air CO₂ flux

565 Seasonal variation in air-sea fluxes is clearly seen in the climatology (Figure 6) and are attributed to a combination of effects including fluctuations in SSTs, biological uptake of carbon dioxide, as well as mixing and wind speeds.

The seasonal variability of fluxes in higher latitudes of the subtropics in the Atlantic, Indian and Pacific Oceans cause an oscillation from neutral or weak sources of CO₂ to the atmosphere in the warmer seasons to strong CO₂ sinks in the cooler or winter
570 seasons. Water cools as it is transported poleward by western boundary currents, allowing for carbon uptake (Ayers & Lozier 2012). In spring and summer, the biological

drawdown of carbon increases CO₂ uptake by the ocean, partially offset by increases in fCO₂ due to warming.

575 Subtropical gyre regions also transition from weak sinks in the winter seasons to weak
sources in the summer seasons, following the seasonal SST cycles and reflecting the
dominance of temperature effects in controlling the seasonal variability in the fCO₂ and
sea–air fluxes in oligotrophic gyres. In tropical low latitude regions, seasonality is
580 generally smaller, however localized hot spots of high variability and large fluxes do
exist, such as in the northwestern Indian Ocean where the strong summer monsoon
winds force upwelling of carbon rich subsurface waters and cause high gas transfer
rates in this region (Chen and Tsunogai 1998, T-2002, Sabine et al. 2000). The
equatorial Pacific and Atlantic show little seasonal variability in CO₂ flux with a
persistent efflux throughout the year.



585 Figure 6: Seasonal sea–air CO₂ flux (molC m⁻² year⁻¹) climatology for (a) December, January, February (DJF) and (b) June, July, August (JJA). Positive values (warm colors)

indicate sea-to-air fluxes (ocean efflux), and negative values (cool colors) indicate air-to-sea fluxes (ocean uptake).

590

In the Southern Ocean, there is a consistent region of moderate carbon source waters located in the Atlantic and Indian sector south of 45S latitude during the austral winter (Figure 6b). The source in the Southern Ocean region could be influenced by high $f\text{CO}_2$ waters from margins of the Antarctic sea-ice field given that the efflux values occur during the austral winter months (JJA). As the seasons transition to warmer temperatures and the ice edge recedes, this region is impacted by high rates of photosynthesis causing $f\text{CO}_2$ drawdown, and resulting in a transition to moderate carbon sinks during the austral summer (DJF). Another possibility is that the austral winter carbon source is linked to deep mixing and/or upwelling water which would bring an import of high DIC to the surface layers. Given the limited number of observations, particularly in winter in the Southern Ocean (Figure 1), confidence in the resulting climatology is lower in this region.

595

600

5. Discussion

It should be noted that there isn't one specific reference year for this release of the $\Delta f\text{CO}_2$ climatology as was the case for previous releases (e.g., the year 2000 reference in T-2009). Instead, this climatology represents a multidecadal time period, beginning in 1980, with the majority of observations feeding into the climatology collected after 2010. Therefore, while the $\Delta f\text{CO}_2$ climatology is not reported for a specific reference year, it is most representative of the conditions over the past two decades. We note however that the flux estimates given in this analysis are based on inputs from a single year, the year 2010, as described above in Section 3.3 (comparison of flux estimates using 2010 inputs and averages over several decades yield very similar results, also as described in Section 3.3).

605

610

615 5.1 Comparison with T-2009 climatology

In the previous release of this climatology (T-2009), $p\text{CO}_2$ values were corrected to a reference year of 2000 using a mean atmospheric CO_2 increase rate of $1.5 \mu\text{atm yr}^{-1}$ over the entire ocean area with the exception of the Bering Sea, where the observed rate of $-1.2 \mu\text{atm yr}^{-1}$ was used. In our updated method described above (Section 3.1), we eliminate the need to apply a normalization rate for observations and instead calculate a $\Delta f\text{CO}_2$ value for each observation using a co-located concurrent atmospheric $f\text{CO}_2$ value. We note that T-2014 presents a more updated $p\text{CO}_2$ climatology than T-

620

2009. Since T-2014 emphasizes climatologies for the other carbonate system variables
625 (pH, dissolved inorganic carbon, and total alkalinity) and omits estimation of fluxes, we
focus our comparison on values presented in T-2009.

Spatial differences between the climatology created from surface water $\Delta f\text{CO}_2$ values
using the methods discussed above and the approach of T-2009 (3 million
630 observations) are shown in Figure 7 for months February and August- months were
selected for consistency with past comparisons presented in T-2009 and T-2002. The
differences between this updated release and previous versions producing climatologies
for reference years 2000 (T-2009) and 1990 (T-1997) are unlikely to represent real
change in the oceans over time, but instead primarily reflect the impact of the greatly
635 expanded database as well as the use of the $\Delta f\text{CO}_2$ approach as opposed to the time
normalization method of T-2009 (Supplementary Figure 9).

The most significant regional differences between this updated version and that of T-
2009 are observed over the subpolar North Atlantic, the subtropical Southeast Pacific
640 and portions of the Southern Ocean. In the North Atlantic, differences between versions
are largest in the boreal winter (February map, top panel of Figure 7) when the updated
climatology exhibits less uptake compared to the T-2009 version (positive values on the
map indicate more negative values in the T-2009 version). Differences in the North
Atlantic can be at least partially attributed to the much greater availability of
645 observations in this region between the two databases (Figure 1, Supplementary Figure
1, Supplementary Figure 9). This is discussed in further detail in the supplementary text.

The Southeast Pacific is an area with very limited observations but where a few key
datasets have been included in the SOCAT database since 2010. Figure 1 shows that
650 despite these recent additions to SOCAT, there are still only a few observations
covering this region. Comparison of Figure 3 in this study with Figure 9 of T-2009
suggests that the additional datasets in SOCATv2022 result in a more defined seasonal
cycle for $f\text{CO}_2$ in the subtropical Southeast Pacific in the current release. Specifically,
the map of differences shown in Figure 7 shows that this region is a greater source of
655 carbon to the atmosphere in austral summer and a greater sink in austral winter
compared to T-2009 (compare also Figure 6 of this study with Figure 15 of T-2009). In
contrast, monthly maps included in Figure 3 of T-2009 show little seasonal contrast in
 $\Delta p\text{CO}_2$ likely due to a lack of observations.

660 In the Southern Ocean region during austral winter (August), $\Delta f\text{CO}_2$ values are more
negative in the current version compared to T-2009. The Southern Ocean is also a
region of limited data availability particularly in austral winter but one where

SOCATv2022 also includes several datasets added in the past decade that have an outsized influence on the resulting climatology.

665

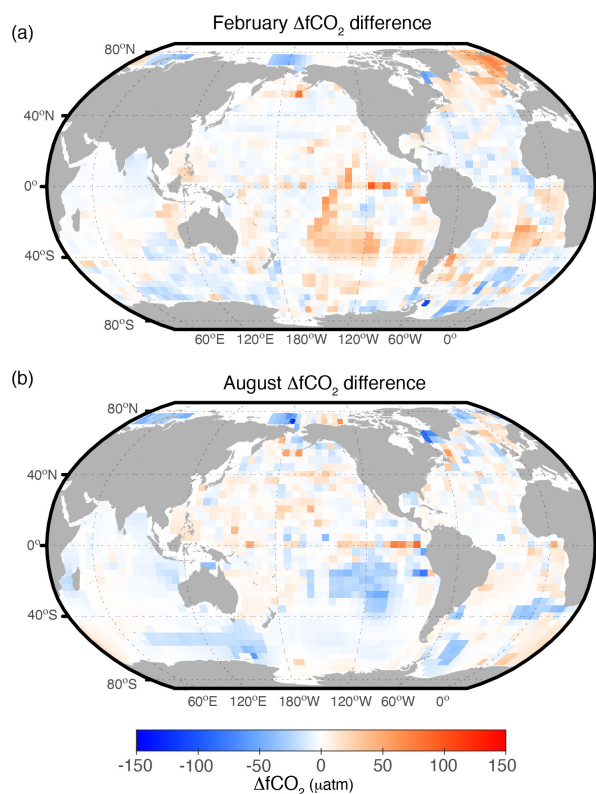


Figure 7: Difference maps for the surface water $\Delta f\text{CO}_2$ climatology produced by this study using SOCAT and that from T-2009 (maps show this study *minus* T-2009) in (a) February and (b) August. In T-2009, the delta CO_2 values are reported as $p\text{CO}_2$ and here we are using $f\text{CO}_2$.

670

5.2 Comparison to other flux estimates

The estimate presented here for annual global mean carbon flux ($-1.79 \text{ PgC yr}^{-1}$) represents slightly less uptake than reported by other studies, but given uncertainties, as well as differing timeframes, spatial coverage and gap-filling methodologies, our estimate compares closely with current estimates similarly based on observed surface ocean $f\text{CO}_2$.

675

To compare our new climatological estimate of contemporary air–sea net flux from surface ocean $f\text{CO}_2$ with estimates of the anthropogenic carbon flux from interior data (e.g., Gruber et al. 2019) or estimates from global ocean biogeochemical models (e.g., Friedlingstein et al. 2022; Hauck et al. 2020), it is necessary to account for the

680

685 outgassing of natural carbon supplied to the ocean by rivers. This riverine estimate
varies significantly in magnitude between studies and continues to be a research focus
for the ocean carbon community. Therefore, we focus on comparisons between our
climatological estimate and a mean carbon flux estimate from an ensemble of
observation-based pCO₂ products included in the SeaFlux product (Fay & Gregor et al.
2021).

690 The SeaFlux products span the years 1985-2020, are all similarly based on the SOCAT
database, but employ various methods of machine learning and interpolation to produce
full coverage ocean carbon maps. For this comparison, a climatology of the SeaFlux
product is produced and fluxes are calculated in the same manner as for the climatology
695 presented here. Following this approach, the SeaFlux climatology ensemble yields a
global mean flux of -2.10 PgC yr⁻¹ which represents a slightly larger flux into the ocean
than that produced by the updated climatology (-1.79 ± 0.7 PgC yr⁻¹). The differences in
global flux can be attributed to the true global coverage of the SeaFlux product relative
to the 90% global ocean coverage of this study. As mentioned above in Section 4.2, an
700 estimate of missing coastal and high latitude fluxes increases the ocean carbon uptake
estimate for this climatology by roughly 0.38 PgC yr⁻¹. Adding this additional flux brings
our analysis within 0.1 PgC yr⁻¹ of the SeaFlux ensemble (-2.17 PgC yr⁻¹ versus -2.10
PgC yr⁻¹ for this analysis versus the SeaFlux estimate, respectively).

705 Spatially, comparison of the SeaFlux ensemble of products to our climatology shows
strong agreement in overall patterns but significant differences in the mid and high
latitude Southern Hemisphere oceans (Figure 8). Gloege et al. (2021) analyzed a
machine learning method's ability to reconstruct global carbon fluxes from available
observations using a testbed approach and found the highest flux bias in the Southern
710 Ocean regions as well as an overestimation of decadal variability in this region. Given
the limited availability of year-round observations at high Southern Hemisphere
latitudes, and the resulting reliance on various gap-filling approaches, it is not surprising
that the largest differences between the climatology presented here and the SeaFlux
ensemble emerges in this region. Significant differences between these climatologies
715 are also evident in the high latitude North Pacific and North Atlantic, specifically in the
boreal winter season (Figure 8a). Again, a lack of observations in these regions during
the winter season (Figure 1) likely accounts for much of this disagreement, with more
reliance on the interpolation methods used by each method. Machine learning methods
that utilize proxy variables to estimate pCO₂ in unsampled areas, such as those in the
720 SeaFlux product, often rely on relationships derived from better-observed areas that are
deemed similar in biogeochemical characteristics and it is likely that the mechanisms at
these high latitude locations are not accurately captured by any available interpolation

methods. This is also a current focus of research for the ocean carbon observing community.

725

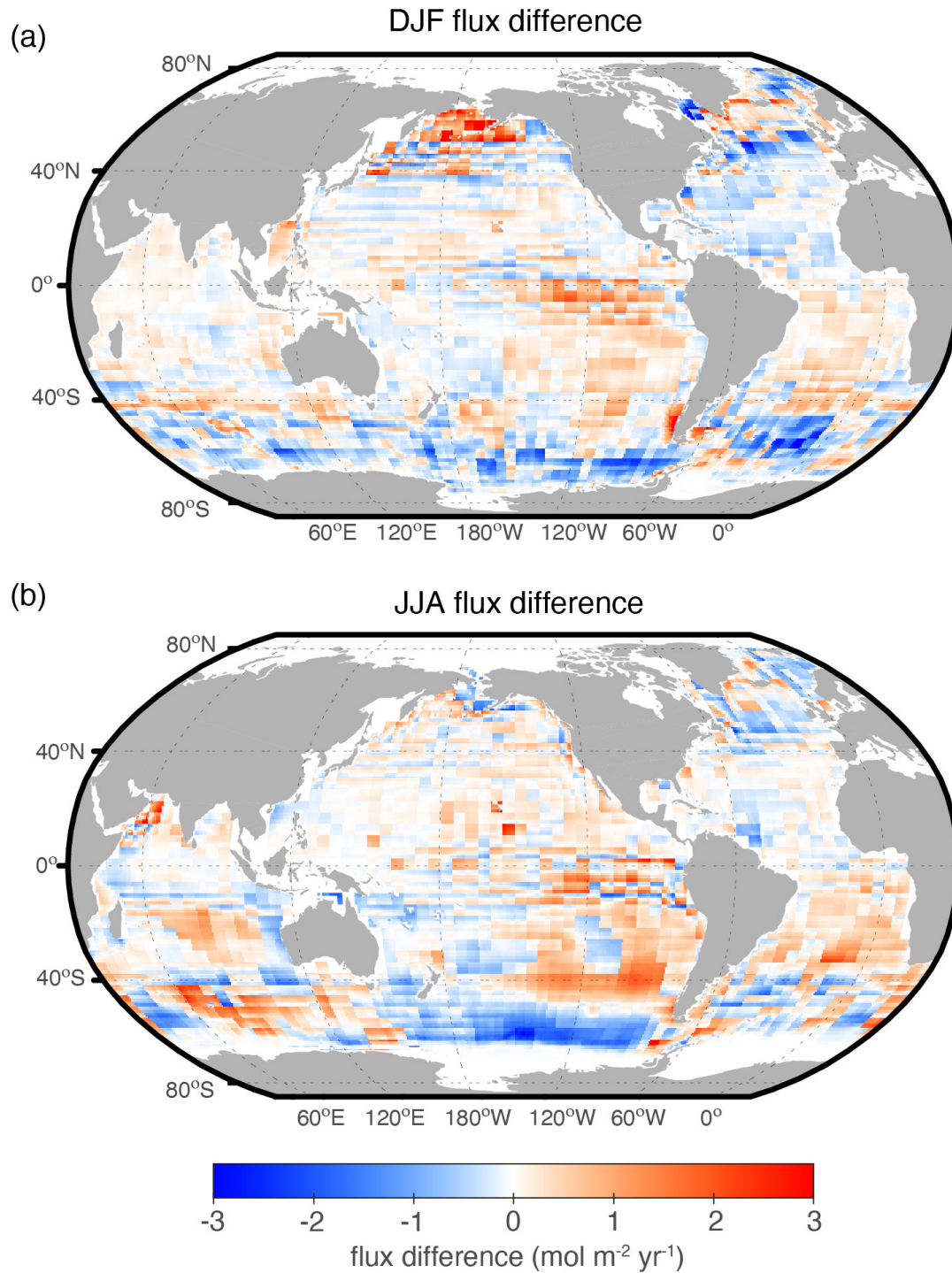


Figure 8: Difference map for carbon fluxes ($\text{mol m}^{-2} \text{yr}^{-1}$) calculated from this ΔfCO_2 climatology and fluxes reported by an ensemble of observation-based products included

730 in the SeaFlux product for (a) boreal winter, DJF and (b) boreal summer, JJA. Map
shows the difference defined as this study *minus* SeaFlux. Note that white areas at the
poles are due to ice coverage extent (and therefore no value reported in the
climatology) and not a flux difference of 0.

6. Conclusion

735 An updated climatological mean distribution for $\Delta f\text{CO}_2$ (surface water minus
atmosphere) using the methods of T-2009 is presented. This climatology is based on
approximately seven times more open ocean observations from the SOCATv2022
database (over 21 million values, spanning years 1980-2021) compared to the 3 million
740 data values used in T-2009 (and more than three times the approximately 6.5 million
observations used in T-2014). In this updated climatology, observations made during El
Niño periods over the equatorial Pacific are included, unlike climatologies presented by
T-1997, T-2002, T-2009 and T-2014. In addition to coastal waters, the highest latitudes
of the Arctic and the Mediterranean Sea are also excluded as in all previous LDEO
climatologies.

745 To develop a climatology from data collected over multiple decades during which $f\text{CO}_2$
experienced a large secular trend, we calculate $\Delta f\text{CO}_2$ values for each day and grid cell
before collapsing all available data onto one climatological year. This method follows
the assumption made in previous iterations of this climatology (T-1997) that the ocean
750 surface carbon value follows the rate of increase in the atmospheric $f\text{CO}_2$, such that
 $\Delta f\text{CO}_2$ is constant over time. Observed $\Delta f\text{CO}_2$ is then interpolated in space-time using a
lateral two-dimensional diffusion–advection equation on a $4^\circ \times 5^\circ$ grid (Takahashi et al.
1995, T-1997, T-2002, T-2009, T-2014). Monthly mean $\Delta f\text{CO}_2$ values for each pixel,
downscaled to $1^\circ \times 1^\circ$ resolution, are presented here. Net sea-air CO_2 flux is computed
755 using the pySeaFlux package, following the protocol presented in Fay & Gregor et al.
(2021).

Regional mean $\Delta f\text{CO}_2$ values vary greatly among the ocean basins (Figures 3 and 4).
The high-latitude North Atlantic is the most intense CO_2 sink per unit area as a result of
760 both highly negative $\Delta f\text{CO}_2$ (Figure 3) and strong winds. This is also the region with the
largest differences between the climatologies created with previous versions of the
LDEO database and this version based on the SOCATv2022 database (Figures 3 and
7). Globally, differences are due to the greater abundance of observations over all
regions of the global oceans in the SOCAT database, but particularly the greater
765 seasonal coverage in the Southern Hemisphere oceans and subpolar North Atlantic
(Figure 1, Supplementary Figure 1).

770 The annual mean uptake flux for the global open-ocean region is estimated to be $-1.79 \pm 0.7 \text{ PgC yr}^{-1}$ for 1980-2021 (Figures 5 and 6). Of the major ocean basins, the Southern Hemisphere ocean (south of 30S) is the largest CO_2 sink, taking up 1.22 PgC yr^{-1} , while the Northern Hemisphere ocean (north of 30N) takes up 0.93 PgC yr^{-1} . The equatorial ocean region acts as the only year-round region of carbon efflux to the atmosphere and emits 0.36 PgC to the atmosphere annually.

775 While over a million new shipboard $f\text{CO}_2^{\text{oce}}$ observations have been made each year in the global oceans for the past two decades, there has been a notable decline in the observations submitted to SOCAT since 2017 (Bakker et al. 2022, 2023). This decline is due in part to the disruption of the COVID19 pandemic, but also reflects a shift away from shipboard $p\text{CO}_2$ measurements. Given the lack of alternative approaches with
780 which to assess spatial and temporal variability in air-sea CO_2 flux and the need for high accuracy shipboard measurements (accuracy of $<2 \mu\text{atm}$) to characterize most regions of the global oceans, this trend to fewer observations is highly detrimental to carbon cycle research. This is true both in regard to monitoring of ocean carbon uptake and to
785 monitoring of more uncertain fluxes such as that between the atmosphere and terrestrial biosphere since the high uncertainty of independent terrestrial estimates necessitates the monitoring of this flux by difference.

790

795 Data Availability

The updated climatology is available via The National Center for Environmental Information (NCEI) at <https://www.ncei.noaa.gov/access/metadata/landing-page/bin/iso?id=gov.noaa.nodc:028225>, doi.org/10.25921/295g-sn13, (Fay et al. 2023).

800 Author contribution

ARF and DRM conducted the analysis and prepared the manuscript. GAM, RW, CW, SCS, and DP contributed ideas and provided feedback throughout the analysis as well as contributed to manuscript.

Acknowledgements

805 The Surface Ocean CO₂ Atlas (SOCAT) is an international effort, endorsed by the
International Ocean Carbon Coordination Project (IOCCP), the Surface Ocean Lower
Atmosphere Study (SOLAS) and the Integrated Marine Biosphere Research (IMBeR)
program, to deliver a uniformly quality-controlled surface ocean CO₂ database. The
810 many researchers and funding agencies responsible for the collection of data and
quality control are thanked for their contributions to SOCAT. Funding was obtained from
the NOAA Office of Oceanic and Atmospheric Research (OAR) Global Ocean
Monitoring and Observations (GOMO) program.

References

- 815 Atlas, R., Hoffman, R. N., Ardizzone, J., Leidner, S. M., Jusem, J.C., Smith, D. K., and
Gombos, D.: A cross-calibrated, multi- platform ocean surface wind velocity product for
meteorological and oceanographic applications, *B. Am. Meteorol. Soc.*, 92, 157– 174,
<https://doi.org/10.1175/2010BAMS2946.1>, 2011.
- Ayers, J.M. and Lozier, M.S., Unraveling dynamical controls on the North Pacific carbon
820 sink. *Journal of Geophysical Research: Oceans*, 117(C1), 2012.
- Bates, N. R., Astor, Y. M., Church, M. J., Currie, K., Dore, J. E., Gonzalez-Davila, M.,
Lorenzoni, L., Muller-Karger, F., Olafsson, J., & Santana-Casiano, J. M., A Time-Series
View of Changing Surface Ocean Chemistry Due to Ocean Uptake of Anthropogenic
825 CO₂ and Ocean Acidification. *Oceanography*, 27(1), 126–141.
<http://www.jstor.org/stable/24862128> 2014.
- Bakker, D. C. E., Pfeil, B. Landa, C. S., Metzl, N., O'Brien, K. M., Olsen, A., Smith, K.,
Cosca, C., Harasawa, S., Jones, S. D., Nakaoka, S., Nojiri, Y., Schuster, U., Steinhoff,
830 T., Sweeney, C., Takahashi, T., Tilbrook, B., Wada, C., Wanninkhof, R., Alin, S. R.,
Balestrini, C. F., Barbero, L., Bates, N. R., Bianchi, A. A., Bonou, F., Boutin, J., Bozec,
Y., Burger, E. F., Cai, W.-J., Castle, R. D., Chen, L., Chierici, M., Currie, K., Evans, W.,
Featherstone, C., Feely, R. A., Fransson, A., Goyet, C., Greenwood, N., Gregor, L.,
Hankin, S., Hardman-Mountford, N. J., Harlay, J., Hauck, J., Hoppema, M., Humphreys,
835 M. P., Hunt, C. W., Huss, B., Ibáñez, J. S. P., Johannessen, T., Keeling, R., Kitidis, V.,
Körtzinger, A., Kozyr, A., Krasakopoulou, E., Kuwata, A., Landschützer, P., Lauvset, S.
K., Lefèvre, N., Lo Monaco, C., Manke, A., Mathis, J. T., Merlivat, L., Millero, F. J.,
Monteiro, P. M. S., Munro, D. R., Murata, A., Newberger, T., Omar, A. M., Ono, T.,
Paterson, K., Pearce, D., Pierrot, D., Robbins, L. L., Saito, S., Salisbury, J., Schlitzer,
840 R., Schneider, B., Schweitzer, R., Sieger, R., Skjelvan, I., Sullivan, K. F., Sutherland, S.

C., Sutton, A. J., Tadokoro, K., Telszewski, M., Tuma, M., Van Heuven, S. M. A. C., Vandemark, D., Ward, B., Watson, A. J., Xu, S.: A multi-decade record of high quality fCO₂ data in version 3 of the Surface Ocean CO₂ Atlas (SOCAT). *Earth System Science Data* 8: 383-413. doi:10.5194/essd8-383-2016, 2016.

845

Bakker, D. C. E.; Alin, S. R.; Becker, M.; Bittig, H. C.; Castaño-Primo, R.; Feely, R. A.; Gkritzalis, T.; Kadono, K.; Kozyr, A.; Lauvset, S. K.; Metzl, N.; Munro, D.R.; Nakaoka, S.; Nojiri, Y.; O'Brien, K. M.; Olsen, A.; Pfeil, B.; Pierrot, D.; Steinhoff, T.; Sullivan, K. F.; Sutton, A. J.; Sweeney, C.; Tilbrook, B.; Wada, C.; Wanninkhof, R.; Willstrand Wranne, A.; Akl, J.; Apelthun, L.B.; Bates, N.; Beatty, C.M.; Burger, E. F.; Cai, W.; Cosca, C.E.; Corredor, J.E.; Cronin, M.; Cross, J. N.; De Carlo, E. H.; DeGrandpre, M. D.; Emerson, S. R.; Enright, M. P.; Enyo, K.; Evans, W.; Frangoulis, C.; Fransson, A.; García-Ibáñez, M. I.; Gehrung, M.; Giannoudi, L.; Glockzin, M.; Hales, B.; Howden, S.D.; Hunt, C. W.; Ibáñez, J.S. P.; Jones, S. D.; Kamb, L.; Körtzinger, A.; Landa, C. S.; Landschützer, P.; Lefèvre, N.; Lo Monaco, C.; Macovei, V. A.; Maenner, A.; Jones, S.; Meinig, C.; Millero, F. J.; Monacci, N. M.; Mordy, C.; Morell, J. M.; Murata, A.; Musielewicz, S.; Neill, C.; Newberger, T.; Nomura, D.; Ohman, M.; Ono, T.; Passmore, A.; Petersen, W.; Petihakis, G.; Perivoliotis, L.; Plueddemann, A. J.; Rehder, G.; Reynaud, T.; Rodriguez, C.; Ross, A. C.; Rutgersson, A.; Sabine, C. L.; Salisbury, J. E.; Schlitzer, R.; Send, U.; Skjelvan, I.; Stamatakis, N.; Sutherland, S.C.; Tadokoro, K.; Tanhua, T.; Telszewski, M.; Trull, T.; Vandemark, D.; van Ooijen, E.; Voynova, Y. G.; Wang, H.; Weller, R. A.; Whitehead, C.s; Wilson, D. (2022). Surface Ocean CO₂ Atlas Database Version 2022 (SOCATv2022) (NCEI Accession 0253659). NOAA National Centers for Environmental Information. Dataset. <https://doi.org/10.25921/1h9f-nb73>. Accessed July 14, 2022.

850

855

860

865

Bakker, D., Sanders, R., Collins, A., DeGrandpre, M., Gkritzalis, T., Ibáñez, S., Jones, S., Lauvset, S., Metzl, N., O'Brien, K., Olsen, A., Schuster, U., Steinhoff, T., Telszewski, M., Tilbrook, B., Wallace, D.: Case for SOCAT as an integral part of the value chain advising UNFCCC on ocean CO₂ uptake http://www.ioccp.org/images/Gnews/2023_A_Case_for_SOCAT.pdf, 2023

870

Chen, C. T. A., and S. Tsunogai. "Carbon and nutrients in the ocean." *Asian Change in the Context of Global Change*: 271-307, 1998.

875

DeVries T., Yamamoto K., Wanninkhof R., Gruber N., Hauck J., Müller J.D., Bopp L., Carroll D., Carter B., Chau T., Doney S., Gehlen M., Gloege L., Gregor L., Henson S., Kim J.H., Iida Y., Ilyina T., Landschützer P., Le Quéré C., Munro D., Nissen C., Patara L., Perez F.F., Resplandy L., Rodgers K., Schwinger J., Séférian R., Sicardi V., Terhaar J., Triñanes J., Tsujino H., Watson A., Yasunaka S., Zeng, J.: Magnitude, trends, and variability of the global ocean carbon sink from 1985-2018, *Global Biogeochemical Cycles*, 37, e2023GB007780. <https://doi.org/10.1029/2023GB007780>, 2023.

- 880 Dickson, A. G., Sabine, C. L., and Christian, J. R. (Eds.): Guide to best practices for ocean CO₂ measurements, PICES Special Publication 3, IOCCP Report 8, 191 pp., 2007.
- Fay, A.R. and McKinley, G.A.: Global trends in surface ocean pCO₂ from in situ data. *Global Biogeochemical Cycles*, 27(2), pp.541-557, 2013.
- 885 Fay, A. R., & McKinley, G. A.: Global open-ocean biomes: Mean and temporal variability. *Earth System Science Data*, 6(2), 273–284. <https://doi.org/10.5194/essd-6-273-2014>, 2014.
- 890 Fay, A. R., Gregor, L., Landschützer, P., McKinley, G. A., Gruber, N., Gehlen, M., Iida, Y., Laruelle, G. G., Rödenbeck, C., Roobaert, A., and Zeng, J.: SeaFlux: harmonization of air–sea CO₂ fluxes from surface pCO₂ data products using a standardized approach, *Earth Syst. Sci. Data*, 13, 4693–4710, <https://doi.org/10.5194/essd-13-4693-2021>, 2021
- 895 Fay, A. R., Munro, D.R., McKinley, G. A., Pierrot, D., Sutherland, S. C., Sweeney, C., Wanninkhof, R.: Climatological distributions of sea-air Delta fCO₂ and CO₂ flux densities in the Global Surface Ocean (NCEI Accession 0282251). NOAA National Centers for Environmental Information. Dataset. <https://doi.org/10.25921/295g-sn13>, 2023.
- 900 Feng, S., Lauvaux, T., Keller, K., Davis, K. J., Rayner, P., Oda, T., and Gurney, K. R.: A road map for improving the treatment of uncertainties in high-resolution regional carbon flux inverse estimates, *Geophysical Research Letters*, 46, 13,461–13,469. <https://doi.org/10.1029/2019GL082987>, 2019.
- 905 Friedlingstein, P., O'Sullivan, M., Jones, M. W., Andrew, R. M., Gregor, L., Hauck, J., Le Quéré, C., Luijkx, I. T., Olsen, A., Peters, G. P., Peters, W., Pongratz, J., Schwingshackl, C., Sitch, S., Canadell, J. G., Ciais, P., Jackson, R. B., Alin, S. R., Alkama, R., Arneeth, A., Arora, V. K., Bates, N. R., Becker, M., Bellouin, N., Bittig, H. C.,
- 910 Bopp, L., Chevallier, F., Chini, L. P., Cronin, M., Evans, W., Falk, S., Feely, R. A., Gasser, T., Gehlen, M., Gkritzalis, T., Gloege, L., Grassi, G., Gruber, N., Gürses, Ö., Harris, I., Hefner, M., Houghton, R. A., Hurtt, G. C., Iida, Y., Ilyina, T., Jain, A. K., Jersild, A., Kadono, K., Kato, E., Kennedy, D., Klein Goldewijk, K., Knauer, J., Korsbakken, J. I., Landschützer, P., Lefèvre, N., Lindsay, K., Liu, J., Liu, Z., Marland, G., Mayot, N., McGrath, M. J., Metzl, N., Monacci, N. M., Munro, D. R., Nakaoka, S.-I., Niwa, Y., O'Brien, K., Ono, T., Palmer, P. I., Pan, N., Pierrot, D., Pockock, K., Poulter, B., Resplandy, L., Robertson, E., Rödenbeck, C., Rodriguez, C., Rosan, T. M., Schwinger, J., Séférian, R., Shutler, J. D., Skjelvan, I., Steinhoff, T., Sun, Q., Sutton, A. J.,

- 920 Sweeney, C., Takao, S., Tanhua, T., Tans, P. P., Tian, X., Tian, H., Tilbrook, B.,
Tsuji, H., Tubiello, F., van der Werf, G. R., Walker, A. P., Wanninkhof, R., Whitehead,
C., Willstrand Wranne, A., Wright, R., Yuan, W., Yue, C., Yue, X., Zaehle, S., Zeng, J.,
and Zheng, B.: Global Carbon Budget 2022, *Earth Syst. Sci. Data*, 14, 4811–4900,
<https://doi.org/10.5194/essd-14-4811-2022>, 2022.
- 925 Gloor, M., McKinley, G. A., Landschutzer, P., Fay, A. R., Frolicher, T., Fyfe, J., Ilyina,
T., Jones, S., Lovenduski, N. S., Rödenbeck, C., Rogers, K., Schlunegger, S., and
Takano, Y.: Quantifying errors in observationally-based estimates of ocean carbon sink
variability, *Global Biogeochem. Cy.*, 35, e2020GB006788,
<https://doi.org/10.1029/2020GB006788>, 2021.
- 930 Good, S. A., Martin, M. J., and Rayner, N. A.: EN4: Quality controlled ocean
temperature and salinity profiles and monthly objective analyses with uncertainty
estimates, *J. Geophys. Res.-Oceans*, 118, 6704–6716,
<https://doi.org/10.1002/2013JC009067>, 2013.
- 935 Gregor, L., & Fay, A. R.: SeaFlux data set: harmonised sea-air CO₂ fluxes from surface
pCO₂ data products using a standardised approach (2021.04, Data set: Zenodo.
<https://doi.org/10.5281/zenodo.5148460>, 2021. Last accessed September, 12, 2022.
- 940 Gruber, N., Clement, D., Carter, B. R., Feely, R. A., van Heuven, S., Hoppema, M., et
al.: The oceanic sink for anthropogenic CO₂ from 1994 to 2007. *Science* 363, 1193–
1199. doi: 10.1126/science.aau5153, 2019.
- 945 Gruber, N., Bakker, D. C., DeVries, T., Gregor, L., Hauck, J., Landschützer, P., ... &
Müller, J. D.: Trends and variability in the ocean carbon sink. *Nature Reviews Earth &
Environment*, 4(2), 119-134, 2023.
- 950 Hauck, J., Zeising, M., Le Quéré, C., Gruber, N., Bakker, D. C. E., Bopp, L., Chau, T. T.
T., Gürses, Ö., Ilyina, T., Landschützer, P., Lenton, A., Resplandy, L., Rödenbeck, C.,
Schwinger, J., and Séférian, R.: Consistency and Challenges in the Ocean Carbon Sink
Estimate for the Global Carbon Budget, *Front. Mar. Sci.*, 7, 852-885,
<https://doi.org/10.3389/fmars.2020.571720>, 2020.
- 955 Hersbach, H., Bell, B., Berrisford, P., Hirahara, S., Horányi, A., Muñoz-Sabater, J.,
Nicolas, J., Peubey, C., Radu, R., Schepers, D., Simmons, A., Soci, C., Abdalla, S.,
Abellan, X., Balsamo, G., Bechtold, P., Biavati, G., Bidlot, J., Bonavita, M., De Chiara,
G., Dahlgren, P., Dee, D., Diamantakis, M., Dragani, R., Flemming, J., Forbes, R.,
Fuentes, M., Geer, A., Haimberger, L., Healy, S., Hogan, R.J., Hólm, E., Janisková, M.,
Keeley, S., Laloyaux, P., Lopez, P., Lupu, C., Radnoti, G., de Rosnay, P., Rozum, I.,

- 960 Vamborg, F., Villaume, S., and Thépaut, J.: The ERA5 global reanalysis, *Q. J. Roy. Meteor. Soc.* 146, 1999–2049, <https://doi.org/10.1002/qj.3803>, 2020 (data available at: <https://cds.climate.copernicus.eu/cdsapp#!/dataset/reanalysis-era5-single-levels-monthly-means?tab=overview>, last access: 16 October, 2020).
- 965 Jacobson, A. R., Mikaloff-Fletcher, S. E., Gruber, N., Sarmiento, J. S., and Gloor, M.: A joint atmosphere-ocean inversion for surface fluxes of carbon dioxide: 1. Methods and global-scale fluxes, *Glob. Biogeochem. Cy.*, 21, GB1019, doi:10.1029/2005GB002556, 2007.
- 970 Ho, D. T., Wanninkhof, R., Schlosser, P., Ullman, D. S., Hebert, D., and Sullivan, K. F.: Towards a universal relationship between wind speed and gas exchange: Gas transfer velocities measured with $^3\text{He}/\text{SF}_6$ during the Southern Ocean Gas Exchange Experiment, *J Geophys. Res.*, 116, C00F04, doi:10.1029/2010JC006854, 2011.
- 975 Kalnay, E., Kanamitsu, M., Kistler, R., Collins, W., Deaven, D., Gandin, L., Iredell, M., Saha, S., White, G., Woollen, J., Zhu, Y., Chelliah, M., Ebisuzaki, W., Higgins, W., Janowiak, J., Mo, K. C., Ropelewski, C., Wang, J., Leetmaa, A., Reynolds, R., Jenne, R., and Joseph, D.: The NCEP/NCAR 40-year reanalysis project, *B. Am. Meteorol. Soc.*, 77, 437–470, 1996.
- 980 Kobayashi, S., Ota, Y., Harada, Y., Ebata, A., Moriya, M., Onoda, H., Onogi, K., Kamahori, H., Kobayashi, C., Endo, H., Miyaoka, K., and Takahashi, K.: The JRA-55 Reanalysis: General Specifications and Basic Characteristics, *J. Meteorol. Soc. Jpn.*, 93, 5–48, <https://doi.org/10.2151/jmsj.2015-001>, 2015.
- 985 Lan, X., Tans, P., Thoning, K., & NOAA Global Monitoring Laboratory. NOAA Greenhouse Gas Marine Boundary Layer Reference - CO₂. [Data set]. NOAA GML. <https://doi.org/10.15138/DVNP-F961>, 2023.
- 990 Landschützer, P., Gruber, N. and Bakker, D.C.: Decadal variations and trends of the global ocean carbon sink. *Global Biogeochemical Cycles*, 30(10), pp.1396-1417, 2016.
- Landschützer, P., Laruelle, G. G., Roobaert, A., and Regnier, P.: A uniform pCO₂ climatology combining open and coastal oceans, *Earth Syst. Sci. Data*, 12, 2537–2553, <https://doi.org/10.5194/essd-12-2537-2020>, 2020.
- 995 Manning, A. C., and Keeling, R. F., Global oceanic and land biotic carbon sinks from the Scripps atmospheric oxygen flask sampling network, *Tellus*, 58B, pp. 95-116, 2006.

- 1000 McKinley, G.A., Fay, A.R., Eddebbbar, Y.A., Gloege, L. and Lovenduski, N.S.: External forcing explains recent decadal variability of the ocean carbon sink. *Agu Advances*, 1(2), p.e2019AV000149, 2020.
- 1005 Pfeil, B., Olsen, A., Bakker, D. C. E., Hankin, S., Koyuk, H., Kozyr, A., Malczyk, J., Manke, A., Metzl, N., Sabine, C. L., Akl, J., Alin, S. R., Bates, N., Bellerby, R. G. J., Borges, A., Boutin, J., Brown, P. J., Cai, W.-J., Chavez, F. P., Chen, A., Cosca, C., Fassbender, A. J., Feely, R. A., González-Dávila, M., Goyet, C., Hales, B., Hardman-Mountford, N., Heinze, C., Hood, M., Hoppema, M., Hunt, C. W., Hydes, D., Ishii, M., Johannessen, T., Jones, S. D., Key, R. M., Körtzinger, A., Landschützer, P., Lauvset, S. K., Lefèvre, N., Lenton, A., Lourantou, A., Merlivat, L., Midorikawa, T., Mintrop, L., Miyazaki, C., Murata, A., Nakadate, A., Nakano, Y., Nakaoka, S., Nojiri, Y., Omar, A.
- 1010 M., Padin, X. A., Park, G.-H., Paterson, K., Perez, F. F., Pierrot, D., Poisson, A., Rios, A. F., Santana-Casiano, J. M., Salisbury, J., Sarma, V. V. S. S., Schlitzer, R., Schneider, B., Schuster, U., Sieger, R., Skjelvan, I., Steinhoff, T., Suzuki, T., Takahashi, T., Tedesco, K., Telszewski, M., Thomas, H., Tilbrook, B., Tjiputra, J., Vandemark, D., Veness, T., Wanninkhof, R., Watson, A. J., Weiss, R., Wong, C. S., Yoshikawa-Inoue, H.: A uniform, quality controlled Surface Ocean CO₂ Atlas (SOCAT) *Earth System Science Data*, 5, 125-143.doi:10.5194/essd-5-125-2013, 2013.
- 1015
- 1020 Quay, P. D., Tilbrook, B., and Wong C. S., Oceanic uptake of fossil fuel CO₂: carbon-13 evidence, *Science*, 256, pp. 74-79, 1992.
- 1025 Reynolds, R. W., Rayner, N. A., Smith, T. M., Stokes, D. C., and Wang, W.: An improved in situ and satellite SST analysis for climate, *J. Climate*, 15, 1609–1625, [https://doi.org/10.1175/1520-0442\(2002\)015<1609:AIISAS>2.0.CO;2](https://doi.org/10.1175/1520-0442(2002)015<1609:AIISAS>2.0.CO;2), 2002 (data available at: <https://psl.noaa.gov/data/gridded/data.noaa.oisst.v2.html>, last access: 26 April 2021).
- 1030 Ridge, S. M., & McKinley, G. A.: Advective Controls on the North Atlantic Anthropogenic Carbon Sink. *Global Biogeochemical Cycles*, 34(7), 1138. <https://doi.org/10.1029/2019gb006457>, 2020.
- 1035 Rödenbeck, C., Bakker, D. C. E., Gruber, N., Iida, Y., Jacobson, A. R., Jones, S., Landschützer, P., Metzl, N., Nakaoka, S., Olsen, A., Park, G.-H., Peylin, P., Rodgers, K. B., Sasse, T. P., Schuster, U., Shutler, J. D., Valsala, V., Wanninkhof, R., and Zeng, J.: Data-based estimates of the ocean carbon sink variability – first results of the Surface Ocean pCO₂ Mapping intercomparison (SOCOM), *Biogeosciences*, 12, 7251–7278, <https://doi.org/10.5194/bg-12-7251-2015>, 2015.

- 1040 Sabine, C. L., Wanninkhof, R., Key, R. M., Goyet, C., & Millero, F. J.: Seasonal CO₂ fluxes in the tropical and subtropical Indian Ocean. *Marine Chemistry*, 72(1), 33–53. [https://doi.org/10.1016/s0304-4203\(00\)00064-5](https://doi.org/10.1016/s0304-4203(00)00064-5), 2000.
- 1045 Sabine, C. L., Hankin, S., Koyuk, H., Bakker, D. C. E., Pfeil, B., Olsen, A., Metzl, N., Kozyr, A., Fassbender, A., Manke, A., Malczyk, J., Akl, J., Alin, S. R., Bellerby, R. G. J., Borges, A., Boutin, J., Brown, P. J., Cai, W.-J., Chavez, F. P., Chen, A., Cosca, C., Feely, R. A., González-Dávila, M., Goyet, C., Hardman-Mountford, N., Heinze, C., Hoppema, M., Hunt, C. W., Hydes, D., Ishii, M., Johannessen, T., Key, R. M., Körtzinger, A., Landschützer, P., Lauvset, S. K., Lefèvre, N., Lenton, A., Lourantou, A., Merlivat, L., Midorikawa, T., Mintrop, L., Miyazaki, C., Murata, A., Nakadate, A., Nakano, Y., Nakaoka, S., Nojiri, Y., Omar, A. M., Padin, X. A., Park, G.-H., Paterson, K., 1050 Perez, F. F., Pierrot, D., Poisson, A., Ríos, A. F., Salisbury, J., Santana-Casiano, J. M., Sarma, V. V. S. S., Schlitzer, R., Schneider, B., Schuster, U., Sieger, R., Skjelvan, I., Steinhoff, T., Suzuki, T., Takahashi, T., Tedesco, K., Telszewski, M., Thomas, H., Tilbrook, B., Vandemark, D., Veness, T., Watson, A. J., Weiss, R., Wong, C. S., and Yoshikawa-Inoue, H.: Surface Ocean CO₂ Atlas (SOCAT) gridded data products, *Earth* 1055 *Syst. Sci. Data*, 5, 145–153, <https://doi.org/10.5194/essd-5-145-2013>, 2013.
- 1060 Takahashi, T., Olafsson, J., Goddard, J.G., Chipman, D.W. and Sutherland, S.C.: Seasonal variation of CO₂ and nutrients in the high-latitude surface oceans: A comparative study. *Global Biogeochemical Cycles*, 7(4), pp.843-878, 1993.
- 1065 Takahashi, T., Takahashi, T. T., & Sutherland, S. C.: An assessment of the role of the North Atlantic as a CO₂ sink. *Philosophical Transactions of the Royal Society of London. Series B: Biological Sciences*, 348(1324), 143-152, 1995.
- 1070 Takahashi, T., Feely, R.A., Weiss, R.F., Wanninkhof, R.H., Chipman, D.W., Sutherland, S.C. and Takahashi, T.T.: Global air-sea flux of CO₂: An estimate based on measurements of sea–air pCO₂ difference. *Proceedings of the National Academy of Sciences*, 94(16), pp.8292-8299, 1997.
- 1075 Takahashi, T., Sutherland, S.C., Sweeney, C., Poisson, A., Metzl, N., Tilbrook, B., Bates, N., Wanninkhof, R., Feely, R.A., Sabine, C. and Olafsson, J.: Global sea–air CO₂ flux based on climatological surface ocean pCO₂, and seasonal biological and temperature effects. *Deep Sea Research Part II: Topical Studies in Oceanography*, 49(9-10), pp.1601-1622, 2002.
- Takahashi, T.: "The fate of industrial carbon dioxide." *Science* 305, no. 5682: 352-353 2004.

1080 Takahashi, T., Sutherland, S.C., Wanninkhof, R., Sweeney, C., Feely, R.A., Chipman,
D.W., Hales, B., Friederich, G., Chavez, F., Sabine, C. and Watson, A., Bakker, D.C.E.,
Schuster U., Metzl, N., Yoshikawa-Inoue, H., Ishii, M., Midorikawa, T., Nojiri, Y.,
Körtzinger, A., Steinhoff, T., Hoppema, M., Olafsson, J., Arnarson, T.S., Tilbrook, B.,
Johannessen, T., Olsen, A., Bellerby, R., Wong, C.S., Delille, B., Bates, N.R., de Baar,
1085 H.J.W.: Climatological mean and decadal change in surface ocean pCO₂, and net sea–
air CO₂ flux over the global oceans. *Deep Sea Research Part II: Topical Studies in
Oceanography*, 56(8-10), pp.554-577, <http://dx.doi.org/10.1016/j.dsr2.2008.12.009>.
2009a.

1090 Takahashi, T., Sutherland, S.C., Wanninkhof, R., Sweeney, C., Feely, R.A., Chipman,
D.W., Hales, B., Friederich, G., Chavez, F., Sabine, C. and Watson, A., Bakker, D.C.E.,
Schuster U., Metzl, N., Yoshikawa-Inoue, H., Ishii, M., Midorikawa, T., Nojiri, Y.,
Körtzinger, A., Steinhoff, T., Hoppema, M., Olafsson, J., Arnarson, T.S., Tilbrook, B.,
Johannessen, T., Olsen, A., Bellerby, R., Wong, C.S., Delille, B., Bates, N.R., de Baar,
1095 H.J.W.: Corrigendum to “Climatological mean and decadal change in surface ocean
pCO₂, and net sea–air CO₂ flux over the global oceans.” *Deep Sea Research Part I:
Oceanographic Research Papers*, 56(11), pp.2075-2076,
<https://doi.org/10.1016/j.dsr.2009.07.007>, 2009b.

1100 Takahashi, T., S. C. Sutherland, D. W. Chipman, J. G. Goddard, C. Ho, T. Newberger,
C. Sweeney, and D. R. Munro: Climatological distributions of pH, pCO₂, total CO₂,
alkalinity, and CaCO₃ saturation in the global surface ocean, and temporal changes at
selected locations, *Mar. Chem.*, 164, 95–125, doi:10.1016/j.marchem.2014.06.004,
2014.

1105 Takahashi, T.; Sutherland, S. C.; Kozyr, A.: Global Ocean Surface Water Partial
Pressure of CO₂ Database: Measurements Performed During 1957-2019 (LDEO
Database Version 2019) (NCEI Accession 0160492). Version 9.9. NOAA National
Centers for Environmental Information. Dataset.
[https://doi.org/10.3334/CDIAC/OTG.NDP088\(V2015\)](https://doi.org/10.3334/CDIAC/OTG.NDP088(V2015)) Accessed March 15, 2021.

1110 Tanhua, T., Orr, J. C., Lorenzoni L., and Hansson L.: WMO Bulletin n° : Vol 64 (1) -
2015 (available at [https://public.wmo.int/en/resources/bulletin/monitoring-ocean-carbon-
and-ocean-acidification-0](https://public.wmo.int/en/resources/bulletin/monitoring-ocean-carbon-and-ocean-acidification-0)), 2015.

1115 Tans, P.p, Fung, I.Y., Takahashi, T., Observational Constrains on the Global
Atmospheric Co₂ Budget. *Science* 247, 1431-1438. DOI:10.1126/science.247.4949.1431,
1990.

1120 Tans, P.P., Berry, J.A., Keeling, R.F.: Oceanic ¹³C/¹²C observations: a new window on ocean CO₂ uptake. *Global Biogeochemical Cycles* 7.2: 353-368, 1993.

1125 Tjiputra, J.F., Olsen, A., Bopp, L., Lenton, A., Pfeil, B., Roy, T., Segschneider, J., Totterdell, I., Heinze, C.: Long-term surface pCO₂ trends from observations and models, *Tellus B: Chemical and Physical Meteorology*, 66:1, 23083, DOI: 10.3402/tellusb.v66.23083, 2014.

1130 Wanninkhof, R., Park, G.-H., Takahashi, T., Sweeney, C., Feely, R., Nojiri, Y., Gruber, N., Doney, S. C., McKinley, G. A., Lenton, A., Le Quéré, C., Heinze, C., Schwinger, J., Graven, H., and Khatiwala, S.: Global ocean carbon uptake: magnitude, variability and trends, *Biogeosciences*, 10, 1983–2000, <https://doi.org/10.5194/bg-10-1983-2013>, 2013.

1135 Wanninkhof R.: Relationship between wind speed and gas exchange over the ocean revisited, *Limnol. Oceanogr. Methods*, 12, doi:10.4319/lom.2014.12.351, 2014.

Weiss, R.: Carbon dioxide in water and seawater: the solubility of non-ideal gas, *Mar. Chem.* 2, 203–215, [https://doi.org/10.1016/0304-4203\(74\)90015-2](https://doi.org/10.1016/0304-4203(74)90015-2), 1974.